

OCCAM

OXFORD CENTRE FOR COLLABORATIVE APPLIED MATHEMATICS

Squeeze-Film Flow in the Presence of a Thin Porous Bed, with Application to the Human Knee Joint

by

D. J. Knox
S. K. Wilson
B. R. Duffy
S. McKee

OCCAM Preprint Number 12/42

SQUEEZE-FILM FLOW IN THE PRESENCE OF A THIN POROUS BED, WITH APPLICATION TO THE HUMAN KNEE JOINT *

D. J. KNOX†, S. K. WILSON‡, B. R. DUFFY§, AND S. MCKEE¶

Abstract. Motivated by the desire for a better understanding of the lubrication of the human knee joint, the squeeze-film flow of a thin layer of Newtonian fluid (representing the synovial fluid) filling the gap between a flat impermeable surface (representing the femoral condyles) and a flat thin porous bed (representing the articular cartilage) coating a stationary flat impermeable surface (representing the tibial plateau) is considered. As the impermeable surface approaches the porous bed under a prescribed constant load all of the fluid is squeezed out of the gap in a finite contact time. In the context of the knee, the size of this contact time suggests that when a person stands still for a short period of time their knees may be fluid lubricated, but that when they stand still for a longer period of time contact between the cartilage-coated surfaces may occur. The fluid particle paths are calculated, and the penetration depths of fluid particles into the porous bed are determined. In the context of the knee, these penetration depths provide a measure of how far into the cartilage nutrients are carried by the synovial fluid, and suggest that when a person stands still nutrients initially in the fluid layer penetrate only a relatively small distance into the cartilage. However, the model also suggests that the cumulative effect of repeated loading and unloading of the knees during physical activity such as walking or running may be sufficient to carry nutrients deep into the cartilage.

Key words. human knee joint, cartilage, synovial fluid, squeeze film, thin film, lubrication, porous bed, finite contact time, particle paths

AMS subject classifications. 76A20, 76D08, 76S05

1. Introduction.

The squeeze-film flow of a thin layer of Newtonian fluid between two impermeable surfaces is a classical problem in fluid mechanics (see, for example, Acheson [1] and Szeri [27]) and it is well known that, at least in theory, an infinite time is required to squeeze the fluid out of the gap between two smooth surfaces (see, for example, Stone [26]). However, in practice, additional physical effects not included in the classical problem (such as, for example, small-scale surface roughness) will inevitably result in contact between the two surfaces in a finite time. Even in theory, the prediction of an infinite contact time is not true for non-smooth surfaces. For example, recently Cawthorn and Balmforth [7] showed that a wedge falling apex-first under gravity through a fluid will make contact with an underlying surface in a finite time. Another situation in which a finite contact time is possible is when fluid is squeezed between porous surfaces. Motivated in part by the fact that classical results were unable to describe the engagement of wet porous clutch plates, Wu [31] considered the squeeze-film flow of a thin layer of fluid between two annular discs, the upper disc being covered with a porous layer. Wu [31] used Reynolds' lubrication theory to describe the flow in the gap between the discs, and Darcy's law to

*The first author (DJK) gratefully acknowledges the financial support of the University of Strathclyde via a University Postgraduate Research Scholarship. Part of this work as undertaken while the corresponding author (SKW) was a Visiting Fellow in the Department of Mechanical and Aerospace Engineering, School of Engineering and Applied Science, Princeton University, USA, and part of it was undertaken while he was a Visiting Fellow in the Oxford Centre for Collaborative Applied Mathematics (OCCAM), Mathematical Institute, University of Oxford, United Kingdom. This publication was based on work supported in part by Award No KUK-C1-013-04, made by King Abdullah University of Science and Technology (KAUST).

† Department of Mathematics and Statistics, University of Strathclyde, 26 Richmond Street, Glasgow G1 1XH, Scotland, United Kingdom. Email: darren.knox@strath.ac.uk

‡ Author for correspondence. Presently also a Visiting Fellow in the Oxford Centre for Collaborative Applied Mathematics (OCCAM), University of Oxford, Mathematical Institute, 24–29 St. Giles', Oxford OX1 3LB. Tel: + 44 (0) 141 548 3820, Fax: + 44 (0) 141 548 3345, Email: s.k.wilson@strath.ac.uk

§ Email: b.r.duffy@strath.ac.uk

¶ Email: s.mckee@strath.ac.uk

describe the flow in the porous layer, and showed that the load-carrying capacity, i.e. the normal force exerted on the discs due to the fluid, is reduced in comparison with the case when both discs are impermeable. Prakash and Vij [20] used a similar model to describe the squeeze-film flow between circular, annular, elliptic and rectangular flat plates, the lower surface being covered with a porous layer. They also used a lubrication approximation for the flow in the porous layer and obtained results similar to those of Wu [31].

A difficulty that arises when using Darcy's law to describe fluid flow in a porous region is that there is, in general, freedom to impose only three of the four "usual" boundary conditions, namely continuity of tangential and normal stresses and continuity of tangential and normal velocities (see, for example, Nield and Bejan [14]) at the interface between the porous region and an adjacent region of fluid. A similar difficulty arises at the interface between a porous region and an impermeable boundary, where it is not, in general, possible to satisfy both no-slip and no-penetration boundary conditions. In most studies the conditions of continuity of normal stress and normal velocity (the latter of which is required to ensure conservation of mass) are imposed at the interface between fluid and porous regions. There is, however, less agreement about which additional boundary condition to impose at such an interface. Some authors (see, for example, Wu [31], Prakash and Vij [20], Goren [10], Nir [16], Sherwood [22], Davis and Hocking [8] and Alleborn and Raszillier [2]) have imposed a condition of no slip relative to the porous solid, so that when the porous solid is stationary the tangential fluid velocity is zero on the fluid side of the interface.

Beavers and Joseph [6] suggested that there is a boundary layer at the interface across which the tangential velocity and the shear stress adjust from their values in the porous region to those in the fluid region. The experiments of Beavers and Joseph [6] suggested that the effect of this boundary layer can be replaced by a slip condition at the interface, now known as the Beavers–Joseph boundary condition. Many authors have used the Beavers–Joseph condition in problems where there is an interface between fluid and porous regions (see, for example, Sherwood [22], Wu [32], Prakash and Vij [21], Lin *et al.* [13], Nield [15] and Nong and Anderson [17]). In squeeze-film problems velocity slip has been found to reduce both the load carrying capacity and the contact time (see, for example, Prakash and Vij [21] and Lin *et al.* [13]).

The difference between the results obtained using the no-slip and the Beavers–Joseph boundary conditions depends on the value of the slip length (see, for example, Sherwood [22] and Prakash and Vij [21]). Sherwood [22] considered thin-film flow in the annular gap between a solid cylinder and a cylindrical wellbore in porous rock. In particular, he calculated the force required to pull the cylinder away from the wellbore when they are initially in contact, and was able to show that velocity slip has a negligible effect on the force if the permeability is small or large.

More general models for the flow in a porous region that allow all four of the usual boundary conditions to be imposed at the interface with an adjacent fluid region have also been used. For example, Lin *et al.* [13] considered an analogous problem to that treated by Wu [31], but with the flow in the porous layer described by the Brinkman model. This model accounts for the effects of viscous shear and thus gives the freedom to impose all four of the usual boundary conditions. Lin *et al.* [13] compared their results with those obtained using Darcy's law with no slip relative to the porous solid and the Beavers–Joseph condition. Reassuringly, they found no dramatic differences between the solutions obtained using the Brinkman model and Darcy's law. For example, results for the fluid layer thickness as a function of time obtained using the Brinkman model were found to lie between those obtained using Darcy's law with no slip relative to the porous solid and the Beavers–Joseph condition.

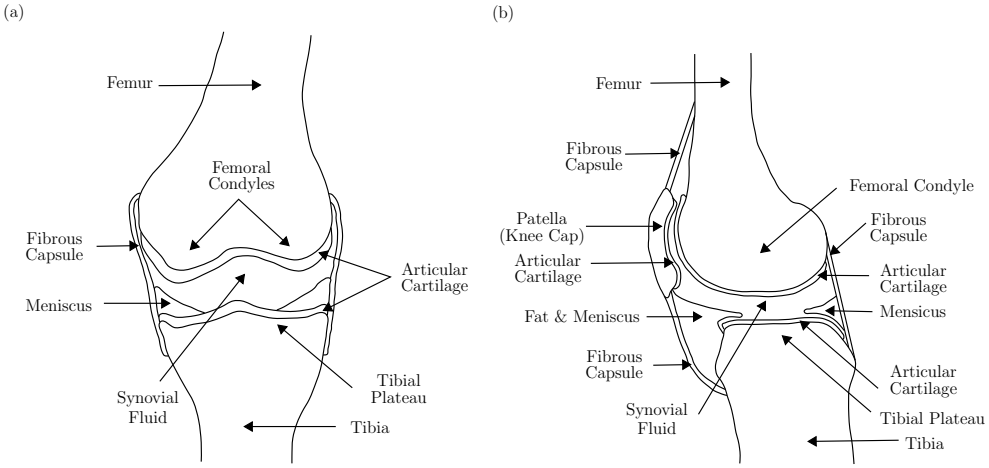

FIG. 1.1. *Sketches of the main anatomical features of the human knee joint. A slice through (a) the front of the knee (behind the patella) and (b) the side of the knee (through the patella)*

Motivated by a desire for a better understanding of, for example, the mechanism by which inhaled particles are removed from the mucus-lined lung wall (Weekley *et al.* [29]), the elastohydrodynamics of the eyelid (Jones *et al.* [12]) and the lubrication of synovial joints (Skotheim and Mahadevan [23]), the effects of deformable surfaces in squeeze-film problems have recently received attention. Weekley *et al.* [29] considered the approach of a parabolic surface towards a flat surface coated with a thin elastic layer through a thin layer of Newtonian fluid. As the fluid pressure increases the thin elastic layer deforms, distributing the pressure over a larger area, and hence slows the approach of the parabolic surface towards the elastic layer. Specifically, Weekley *et al.* [29] showed that the elastic layer deforms in such a way as to create a fluid layer of approximately uniform thickness, with the consequence that the approach is qualitatively the same as that of two flat rigid surfaces. Recently Balmforth *et al.* [5] considered problems related to that treated by Weekley *et al.* [29], the elastic layer being modelled in three different ways, namely as an elastic half-space, as a membrane and as a beam. In each case the presence of the elastic layer was found to slow the approach of the two surfaces, as in the case treated by Weekley *et al.* [29]. Note that, unlike the case of a thin elastic layer treated by Weekley *et al.* [29], none of the models considered by Balmforth *et al.* [5] result in a fluid layer of approximately uniform thickness.

A squeeze film has been proposed as a model for the lubrication of the human knee joint (see, for example, Hou *et al.* [11]). Figure 1.1 shows sketches of the main anatomical features of the human knee joint. The knee is where the largest bones in the human body, the femur and the tibia, meet. Situated at the distal (furthest from the torso) end of the femur are two rounded "knobs" which are referred to as the femoral condyles. When the knee is in flexion or extension the femoral condyles articulate with the tibial plateau which is situated at the proximal (closest to the torso) end of the tibia. Both the femoral condyles and the tibial plateau are coated with a thin layer of articular cartilage, which is a poroelastic material, and the gap between the femoral condyles and the tibial plateau is lubricated by a thin layer of synovial fluid. The latter is a non-Newtonian shear-thinning fluid and has an egg-white-like consistency (see, for example, Fam *et al.* [9] and Balazs [4]). Two crescent-shaped wedges of cartilage, the lateral and medial menisci, are situated on the peripheral boundary of the tibial plateau. The menisci deepen the surface of the tibial plateau,

protecting the underlying articular cartilage and stabilising the joint, and are attached to the fibrous capsule, which is a collection of ligaments that surround the joint, connecting the tibia with the femur, and the patella (knee cap) with both the tibia and the femur. The fibrous capsule prevents the joint from undergoing any abnormal movements, and is lined by the synovial membrane, which secretes and absorbs the synovial fluid that lubricates the joint. The latest (40th) edition of Gray's Anatomy (Standring [24]) contains an excellent overview of the knee.

When a person walks or stands still the force $L = L(t)$ acting through the knee pushes the femoral condyles and the tibial plateau together when $L > 0$, creating a squeeze-film effect, and pulls them apart when $L < 0$. The synovial fluid may be squeezed into or sucked out of the cartilage. Cartilage is avascular (i.e. it does not have a blood supply) and so the flow of synovial fluid into the cartilage is one of the ways that it receives nutrients (see, for example, O'Hara *et al.* [19]). It is believed that when a person walks a thin layer of synovial fluid, reported to be up to 5×10^{-7} m thick (see, for example, Stewart *et al.* [25]), can separate the tibial plateau and the femoral condyles. However, when a person stands still for an extended period of time it is believed that the synovial fluid will eventually be squeezed out of the gap between the tibial plateau and the femoral condyles, and so the cartilage-coated surfaces will eventually come into contact (see, for example, Stewart *et al.* [25]); this is undesirable as it results in cartilage degradation and promotes the onset of osteoarthritis.

As well as being of fundamental scientific and medical interest in its own right, understanding the lubrication of the knee in more detail is of crucial importance in the development of total-knee-replacement technologies (see, for example, Walker *et al.* [28]). In this study we present a simple mathematical model for the human knee joint. For simplicity, both the tibial plateau and the femoral condyles are modelled as rigid impermeable flat surfaces and the effects of the menisci are neglected. Furthermore, for simplicity it is assumed that only the tibial plateau is coated with a thin layer of cartilage, which is modelled as an inelastic porous solid. The thin gap between the tibial plateau and the femoral condyles is filled with, and the pores in the cartilage layer are saturated with, synovial fluid, which is modelled as an incompressible Newtonian fluid. Classical lubrication theory is used to describe the flow of the synovial fluid in the thin gap, and a lubrication approximation to Darcy's law is used to describe the flow of the synovial fluid in the thin cartilage layer. The flows in the two regions are coupled through appropriate boundary conditions at the interface between them. In particular, we impose the Beavers–Joseph condition. We focus on the case of a person standing still, so that the tibial plateau is stationary and the femoral condyles move normally towards it under the action of a prescribed constant load acting though the knee. Note that this is mathematically equivalent to a body with prescribed mass falling under gravity through the fluid region.

At first sight, modelling the femoral condyles as a flat surface appears to be overly simplistic. However, as discussed earlier, the work of Weekley *et al.* [29] shows that when it is approached by a parabolic surface through a thin layer of fluid, a thin elastic layer deforms in such a way as to create a fluid layer of approximately uniform thickness, with the consequence that the approach is qualitatively the same as that of two flat rigid surfaces. Since the femoral condyles are roughly parabolic and cartilage is poroelastic, we anticipate qualitatively similar behaviour in the knee, and thus modelling the femoral condyles as a flat surface is a reasonable first model. Furthermore, assuming that only the tibial plateau is coated with cartilage may also seem overly simplistic. However, when the no-slip condition is used this is mathematically equivalent to both the femoral condyles and the tibial plateau being coated with cartilage layers of half the thickness, and should therefore also give the correct qualitative behaviour for the Beavers–Joseph condition.

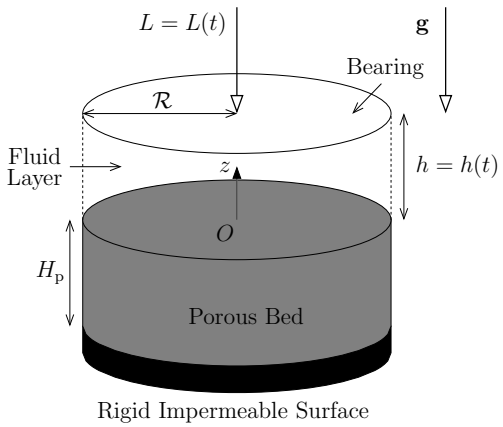

FIG. 2.1. *The geometry of the axisymmetric problem*

The simple mathematical model for the human knee presented in this paper has similarities with some of the models for other physical situations described previously; however, we approach the problem with somewhat different objectives. The aim of our work is to determine the time for which a thin layer of synovial fluid can maintain the separation of the tibial plateau and the femoral condyles when a person stands still (so that there is a prescribed constant load acting through the knee). Furthermore, we are interested in the paths of synovial fluid particles. In particular, we determine the penetration depths of synovial fluid particles into the cartilage layer. This penetration depth provides a measure of how far into the cartilage nutrients are carried by the synovial fluid. The model is solved both numerically and in the asymptotic limits of small and large permeability (corresponding to regimes in which the permeability is much smaller than or much larger than the square of the thickness of the porous layer), the former of which is most relevant to the human knee. In both of these regimes we obtain asymptotic expressions for the contact time and the penetration depth that depend on the model parameters in a relatively simple manner. In particular, we find that at leading order in both limits the contact time and the penetration depth are identical for the no-slip and the Beavers–Joseph boundary conditions.

2. Model Derivation.

2.1. Problem Description. Consider, with reference to the cylindrical polar coordinate system (r, θ, z) shown in Figure 2.1, the time-dependent axisymmetric thin-film flow in the cylindrical gap $0 \leq r \leq \mathcal{R}$, $0 \leq z \leq h$ between a vertically (i.e. in the z-direction) moving circular flat rigid impermeable surface $z = h(t)$ of radius $\mathcal{R}$, representing the femoral condyles, and a stationary circular flat rigid impermeable surface also of radius $\mathcal{R}$ at $z = -H_\mathrm{p}$, representing the tibial plateau, where t denotes time. The tibial plateau is coated with a thin rigid porous layer of constant permeability k, porosity ϕ $(0 < \phi < 1)$ and depth H_p that occupies $0 \leq r \leq \mathcal{R}$, $-H_\mathrm{p} \leq z \leq 0$, representing the thin cartilage layer that coats the tibial plateau. The thin gap between the femoral condyles and the cartilage layer is filled with, and the pores in the cartilage layer are saturated with, synovial fluid, which is modelled as an incompressible Newtonian fluid of constant density ρ and viscosity μ. We prescribe the load $L = L(t) > 0$ that acts vertically downwards through the knee pushing the femoral condyles towards the tibial plateau.

The present model has applications beyond the knee. To make the following presentation as general as possible, henceforth the femoral condyles, the tibial plateau,

the cartilage layer, the fluid-filled gap between the bearing and the porous bed, and the synovial fluid will be referred to as "the bearing", "the rigid impermeable surface", "the porous bed", "the fluid layer", and "the fluid", respectively.

The corresponding two-dimensional problem is also of interest and is therefore treated in Appendix A. In particular, as we show in Appendix A, the solutions for the fluid layer thickness $h = h(t)$ and the fluid particle paths (r, z) may be readily obtained from the corresponding solutions in the axisymmetric case.

2.2. Governing Equations. The axiymmetric flow in the fluid layer ($0 \le r \le \mathcal{R}$, $0 \le z \le h$) is governed by the mass-conservation and Navier–Stokes equations

$$\nabla \cdot \mathbf{v} = 0, \quad \rho\left(\frac{\partial \mathbf{v}}{\partial t} + (\mathbf{v}\cdot\nabla)\mathbf{v}\right) = -\nabla p + \mu\nabla^2\mathbf{v} + \rho\mathbf{g}, \tag{2.1}$$

where $\mathbf{v} = (v_r, 0, v_z)$ is the fluid velocity, with radial and vertical components $v_r = v_r(r, z, t)$ and $v_z = v_z(r, z, t)$, respectively, $p = p(r, z, t)$ is the fluid pressure, and $\mathbf{g} = (0, 0, -g)$ denotes (constant) acceleration due to gravity.

We assume that the axisymmetric flow in the porous bed ($0 \le r \le \mathcal{R}$, $-H_\mathrm{p} \le z \le 0$) is governed by the mass-conservation equation and Darcy's law,

$$\nabla \cdot \mathbf{u} = 0, \quad \mathbf{u} = -\frac{k}{\mu}\nabla P, \tag{2.2}$$

where $\mathbf{u} = (u_r, 0, u_z)$ is the so-called Darcy velocity (the fluid volume flux per unit area), with radial and vertical components $u_r = u_r(r, z, t)$ and $u_z = u_z(r, z, t)$, respectively, and $P = P(r, z, t)$ is the pore pressure. Combining (2.2) shows that P is harmonic, i.e.

$$\nabla^2 P = 0. \tag{2.3}$$

2.3. Equation of Motion of the Bearing. The net force exerted on the bearing by the fluid is in the vertical direction, and is given by

$$F_z = 2\pi \int_0^{\mathcal{R}} \left(p - 2\mu\frac{\partial v_z}{\partial z}\right) r \,\Big|_{z=h} \mathrm{d}r. \tag{2.4}$$

The equation of motion of the bearing is

$$m\frac{\mathrm{d}^2 h}{\mathrm{d}t^2} = F_z - L, \tag{2.5}$$

where m is the mass of the bearing. (In the context of the knee, m would be related to the mass of the person.)

2.4. Boundary and Initial Conditions. On the interface between the bearing and the fluid layer at $z = h$ the no-slip and no-penetration conditions require that

$$v_r = 0, \quad v_z = \frac{\mathrm{d}h}{\mathrm{d}t} \quad \text{on} \quad z = h. \tag{2.6}$$

On the interface between the fluid layer and the porous bed at $z = 0$ mass conservation requires that

$$v_z = u_z \quad \text{on} \quad z = 0, \tag{2.7}$$

while continuity of normal stress requires that

$$-p + 2\mu\frac{\partial v_z}{\partial z} = -P \quad \text{on} \quad z = 0. \tag{2.8}$$

In addition, we impose the Beavers–Joseph condition

$$\frac{k^{1/2}}{\alpha}\frac{\partial v_r}{\partial z} = v_r - u_r \quad \text{on} \quad z = 0, \tag{2.9}$$

where $\alpha\,(>0)$ is the dimensionless Beavers–Joseph constant. This condition allows for velocity slip on the interface between the fluid layer and the porous bed at $z = 0$ with slip length $l_{\rm s} = k^{1/2}/\alpha$. In the limit $\alpha \to \infty$ the slip length $l_{\rm s} \to 0$ and (2.9) reduces to

$$v_r = u_r \quad \text{on} \quad z = 0, \tag{2.10}$$

which corresponds to no slip relative to the fluid at the interface. If we neglect the radial Darcy velocity u_r in (2.10) then the condition becomes

$$v_r = 0 \quad \text{on} \quad z = 0, \tag{2.11}$$

which corresponds to no slip relative to the stationary porous bed.

On the interface between the porous bed and the rigid impermeable surface at $z = -H_{\rm p}$ the no-penetration condition requires that

$$u_z = 0 \quad \text{on} \quad z = -H_{\rm p}. \tag{2.12}$$

At $r = \mathcal{R}$ the pressure in the fluid layer takes the ambient value, which, without loss of generality, we may take to be zero, i.e.

$$p = 0 \quad \text{at} \quad r = \mathcal{R}, \tag{2.13}$$

and, since the fluid pressure is axisymmetric and smooth at $r = 0$, we also require that

$$\frac{\partial p}{\partial r} = 0 \quad \text{at} \quad r = 0. \tag{2.14}$$

Finally, we must also specify the initial thickness of the fluid layer, i.e.

$$h(0) = H_{\rm f}\,(>0). \tag{2.15}$$

In general, solving (2.1), (2.3) and (2.5) would require the specification of additional boundary and initial conditions. However, as we shall show, when both the fluid layer and the porous bed are thin, and a lubrication approximation is used to describe the flow in both of them, the leading order approximations to these equations may, in fact, be solved without specifying any additional conditions.

2.5. Non-dimensionalisation and Lubrication Approximation. We scale and non-dimensionalise the problem as follows:

$$\begin{gathered} r = \mathcal{R}r', \quad z = H_{\rm p}z', \quad t = \frac{\mathcal{R}}{V}t', \quad h = H_{\rm p}h', \quad k = H_{\rm p}^2 k', \\ v_r = Vv_r', \quad v_z = \frac{H_{\rm p}V}{\mathcal{R}}v_z', \quad u_r = Vu_r', \quad u_z = \frac{H_{\rm p}V}{\mathcal{R}}u_z', \\ p = \frac{\mu V\mathcal{R}}{H_{\rm p}^2}p', \quad P = \frac{\mu V\mathcal{R}}{H_{\rm p}^2}P', \quad F_z = \frac{\mu V\mathcal{R}^3}{H_{\rm p}^2}F_z', \quad L = \frac{\mu V\mathcal{R}^3}{H_{\rm p}^2}L', \end{gathered} \tag{2.16}$$

where a prime $'$ denotes a dimensionless variable and $\mathcal{R}$, V, $\mu V\mathcal{R}/H_{\rm p}^2$ and $\mu V\mathcal{R}^3/H_{\rm p}^2$ are characteristic scales for radial distance, radial fluid velocity, pressure and load, respectively.

In dimensionless variables, with the primes omitted for the sake of clarity, the mass-conservation and Navier–Stokes equations (2.1) become

$$\frac{1}{r}\frac{\partial}{\partial r}\left(r v_r\right) + \frac{\partial v_z}{\partial z} = 0, \tag{2.17}$$

$$R^*\left(\frac{\partial v_r}{\partial t} + v_r\frac{\partial v_r}{\partial r} + v_z\frac{\partial v_r}{\partial z}\right) = -\frac{\partial p}{\partial r} + \frac{\partial^2 v_r}{\partial z^2} + O(\epsilon^2), \tag{2.18}$$

$$\epsilon^2 R^*\left(\frac{\partial v_z}{\partial t} + v_r\frac{\partial v_z}{\partial r} + v_z\frac{\partial v_z}{\partial z}\right) = -\frac{\partial p}{\partial z} - G + O(\epsilon^2), \tag{2.19}$$

where the aspect ratio of both the fluid layer and the porous bed, $\epsilon = H_{\mathrm{p}}/\mathcal{R} \ll 1$, the (reduced) Reynolds number for the flow in the fluid layer, $R^* = \epsilon^2\rho V\mathcal{R}/\mu \ll 1$, and the non-dimensional parameter that measures the relative importance of gravitational effects and viscous effects, $G = \epsilon^3\rho g\mathcal{R}^2/\mu V \ll 1$, are all assumed to be small. At leading order in the limit $\epsilon \to 0$ equations (2.18) and (2.19) reduce to the classical lubrication equations

$$\frac{\partial p}{\partial r} = \frac{\partial^2 v_r}{\partial z^2}, \tag{2.20}$$

$$\frac{\partial p}{\partial z} = 0. \tag{2.21}$$

In dimensionless variables, Darcy's law (2.2b) and Laplace's equation (2.3) become

$$\mathbf{u} = (u_r, 0, u_z) = -k\left(\frac{\partial P}{\partial r}, 0, \frac{1}{\epsilon^2}\frac{\partial P}{\partial z}\right), \tag{2.22}$$

$$\frac{1}{r}\frac{\partial}{\partial r}\left(r\frac{\partial P}{\partial r}\right) + \frac{1}{\epsilon^2}\frac{\partial^2 P}{\partial z^2} = 0. \tag{2.23}$$

In dimensionless variables, the equation of motion of the bearing (2.5) becomes

$$I\frac{\mathrm{d}^2 h}{\mathrm{d}t^2} = 2\pi\int_0^1 p\, r\, \mathrm{d}r - L + O(\epsilon^2), \tag{2.24}$$

where the non-dimensional parameter that measures the relative importance of the inertia of the bearing and the vertical forces acting on it, $I = \epsilon^3 mV/\mu\mathcal{R}^2 \ll 1$, is assumed to be small. At leading order in the limit $\epsilon \to 0$ equation (2.24) is simply the load condition

$$L = 2\pi\int_0^1 p\, r\, \mathrm{d}r. \tag{2.25}$$

At leading order in the limit $\epsilon \to 0$ the non-dimensionalised versions of the boundary conditions (2.6)–(2.9) and (2.12)–(2.14) are

$$v_r = 0, \quad v_z = \frac{\mathrm{d}h}{\mathrm{d}t} \quad \text{on} \quad z = h, \tag{2.26}$$

$$v_z = u_z \quad \text{on} \quad z = 0, \tag{2.27}$$

$$P = p \quad \text{on} \quad z = 0, \tag{2.28}$$

$$\frac{k^{1/2}}{\alpha}\frac{\partial v_r}{\partial z} = v_r - \delta u_r \quad \text{on} \quad z = 0, \tag{2.29}$$

$$u_z = 0 \quad \text{on} \quad z = -1, \tag{2.30}$$

$$p = 0 \quad \text{at} \quad r = 1, \tag{2.31}$$

$$\frac{\partial p}{\partial r} = 0 \quad \text{at} \quad r = 0, \tag{2.32}$$

respectively. A new dimensionless parameter δ has been introduced on the right-hand side of (2.29) so that it can be reduced to the non-dimensionalised version of (2.11), i.e. $v_r = 0$ on $z = 0$, by letting $\alpha \to \infty$ and setting $\delta = 0$; otherwise $\delta = 1$. The dimensionless form of the initial condition (2.15) is

$$h(0) = d, \tag{2.33}$$

where we have defined $d = H_{\rm f}/H_{\rm p}$. For simplicity, in all of the plots presented subsequently we take $d = 1$, corresponding to the initial thickness of the fluid layer being the same as the thickness of the porous bed.

2.6. Unsteady Reynolds Equation. Equation (2.21) shows immediately that, since the fluid layer is thin, the leading order fluid pressure is independent of z, i.e. $p = p(r,t)$. Solving the leading order version of (2.23), namely $\partial^2 P/\partial z^2 = 0$, subject to the boundary conditions (2.28) and (2.30) using (2.22) shows that the leading order pore pressure is also independent of z, i.e. $P = P(r,t)$, and hence that at leading order (but not at higher order) the two pressures are the same, i.e. $P(r,t) \equiv p(r,t)$. The variation of P with z appears at first order in ϵ^2, and so seeking a solution to (2.23) in the form

$$P = p(r,t) + \epsilon^2 P_1(r,z,t) + O(\epsilon^4) \tag{2.34}$$

and applying the no-penetration condition (2.30) yields

$$\frac{\partial P_1}{\partial z} = -\frac{(1+z)}{r}\frac{\partial}{\partial r}\left(r\frac{\partial p}{\partial r}\right). \tag{2.35}$$

Substituting (2.34) and (2.35) into (2.22) yields

$$\mathbf{u} = (u_r, 0, u_z) = k\left(-\frac{\partial p}{\partial r}, 0, \frac{(1+z)}{r}\frac{\partial}{\partial r}\left(r\frac{\partial p}{\partial r}\right)\right). \tag{2.36}$$

Solving (2.17) and (2.20) for v_r and v_z subject to the boundary conditions (2.26a), (2.27) and (2.29) using (2.36) yields

$$v_r = -\frac{(h-z)\left[(\alpha h + k^{1/2})z + k^{1/2}(h + 2\delta\alpha k^{1/2})\right]}{2(\alpha h + k^{1/2})}\frac{\partial p}{\partial r}, \tag{2.37}$$

$$v_z = \frac{2(\alpha h + k^{1/2})(6k - z^3) + 3\alpha(h^2 - 2\delta k)z^2 + 6k^{1/2}h(h + 2\delta\alpha k^{1/2})z}{12r(\alpha h + k^{1/2})}\frac{\partial}{\partial r}\left(r\frac{\partial p}{\partial r}\right). \tag{2.38}$$

Substituting (2.38) into (2.26b) we obtain the unsteady Reynolds equation

$$\frac{{\rm d}h}{{\rm d}t} = \frac{h^2(\alpha h^2 + 4k^{1/2}h + 6\delta\alpha k) + 12k(\alpha h + k^{1/2})}{12r(\alpha h + k^{1/2})}\frac{\partial}{\partial r}\left(r\frac{\partial p}{\partial r}\right), \tag{2.39}$$

which, subject to the load condition (2.25), the pressure boundary conditions (2.31) and (2.32), and the initial condition (2.33), determines the pressure $p = p(r,t)$ and the fluid layer thickness $h = h(t)$.

2.7. Streamfunction. The streamfunction $\psi = \psi(r, z, t)$ (non-dimensionalised with $V\mathcal{R}H_{\mathrm{p}}$) satisfies

$$v_r = -\frac{1}{r}\frac{\partial \psi}{\partial z}, \quad v_z = \frac{1}{r}\frac{\partial \psi}{\partial r} \tag{2.40}$$

in the fluid layer $0 \leq z \leq h$, and

$$u_r = -\frac{1}{r}\frac{\partial \psi}{\partial z}, \quad u_z = \frac{1}{r}\frac{\partial \psi}{\partial r} \tag{2.41}$$

in the porous bed $-1 \leq z \leq 0$, and the boundary conditions

$$\psi = 0 \quad \text{on} \quad z = -1, \quad \lim_{z \to 0^+} \psi = \lim_{z \to 0^-} \psi. \tag{2.42}$$

Solving (2.40) and (2.41) for ψ subject to the boundary conditions (2.42) yields

$$\psi = \frac{r\left[2(\alpha h + k^{1/2})(6k - z^3) + 3\alpha(h^2 - 2\delta k)z^2 + 6k^{1/2}h(h + 2\delta\alpha k^{1/2})z\right]}{12(\alpha h + k^{1/2})}\frac{\partial p}{\partial r} \tag{2.43}$$

in the fluid layer $0 \leq z \leq h$, and

$$\psi = kr(1 + z)\frac{\partial p}{\partial r} \tag{2.44}$$

in the porous bed $-1 \leq z \leq 0$.

2.8. Fluid Particle Paths. The path $(r, z) = (r(t), z(t))$ taken by a fluid particle, initially situated at the point (r_0, z_0) (where $0 \leq r_0 \leq 1$ and $-1 \leq z_0 \leq d$) is governed by the ordinary differential equations

$$\frac{\mathrm{d}r}{\mathrm{d}t} = v_r, \quad \frac{\mathrm{d}z}{\mathrm{d}t} = v_z \tag{2.45}$$

in the fluid layer $0 \leq z \leq h$, and

$$\frac{\mathrm{d}r}{\mathrm{d}t} = \frac{u_r}{\phi}, \quad \frac{\mathrm{d}z}{\mathrm{d}t} = \frac{u_z}{\phi} \tag{2.46}$$

in the porous bed $-1 \leq z \leq 0$.

3. General Solution.

3.1. Pressure and Velocities. Integrating the unsteady Reynolds equation (2.39) twice with respect to r and applying the pressure boundary conditions (2.31) and (2.32) we obtain

$$p = -\frac{3(\alpha h + k^{1/2})(1 - r^2)}{h^2(\alpha h^2 + 4k^{1/2}h + 6\delta\alpha k) + 12k(\alpha h + k^{1/2})}\frac{\mathrm{d}h}{\mathrm{d}t}. \tag{3.1}$$

Applying the load condition (2.25) yields a separable first-order ordinary differential equation for the fluid layer thickness $h = h(t)$:

$$L(t) = -\frac{3\pi(\alpha h + k^{1/2})}{2\left[h^2(\alpha h^2 + 4k^{1/2}h + 6\delta\alpha k) + 12k(\alpha h + k^{1/2})\right]}\frac{\mathrm{d}h}{\mathrm{d}t}. \tag{3.2}$$

Re-arranging (3.2) for $\mathrm{d}h/\mathrm{d}t$ and substituting into (3.1) reveals that the pressure is simply

$$p = \frac{2(1-r^2)L(t)}{\pi}, \tag{3.3}$$

showing that the pressure is parabolic in r and independent of k, and that its only temporal dependence is via that of the load $L(t)$. Substituting (3.3) into (2.36) shows that the Darcy velocity is given by

$$\mathbf{u} = (u_r, 0, u_z) = \frac{4L(t)k}{\pi}(r, 0, -2(1+z)), \tag{3.4}$$

which is independent of both α and δ, and so is the same for all three choices of boundary condition (2.9)–(2.11). Substituting (3.3) into (2.37) and (2.38) shows that the fluid velocity is given by $\mathbf{v} = (v_r, 0, v_z)$, where

$$v_r = \frac{2L(t)(h-z)\left[(\alpha h + k^{1/2})z + k^{1/2}(h + 2\delta\alpha k^{1/2})\right] r}{\pi(\alpha h + k^{1/2})}, \tag{3.5}$$

$$v_z = -\frac{2L(t)\left[2(\alpha h + k^{1/2})(6k - z^3) + 3\alpha(h^2 - 2\delta k)z^2 + 6k^{1/2}h(h + 2\delta\alpha k^{1/2})z\right]}{3\pi(\alpha h + k^{1/2})}. \tag{3.6}$$

In particular, (3.4)–(3.6) show that both u_r and v_r are linear in r, but that both u_z and v_z are independent of r.

3.2. Fluid Layer Thickness. Integrating (3.2) from 0 to t and imposing the initial condition (2.33) yields an implicit solution for the fluid layer thickness $h = h(t)$:

$$\int_0^t L(\tau)\,\mathrm{d}\tau = \frac{3\pi}{2}\int_h^d \frac{\alpha s + k^{1/2}}{s^2(\alpha s^2 + 4k^{1/2}s + 6\delta\alpha k) + 12k(\alpha s + k^{1/2})}\,\mathrm{d}s. \tag{3.7}$$

For simplicity in the remainder of the present work we concentrate on the case of constant (dimensional) load $L = L_0 > 0$, corresponding to a person standing still, and choose the characteristic radial fluid velocity scale used in the non-dimensionalisation (2.16) to be $V = L_0 H_{\mathrm{p}}^2/\mu\mathcal{R}^3$, corresponding to taking the constant (dimensionless) load to be equal to unity, i.e. $L_0 = 1$, without loss of generality. We shall, however, retain the constant (dimensionless) load L_0 explicitly in what follows for clarity of presentation.

In the case of constant load $L = L_0$ equation (3.7) yields an explicit expression for the time $t = t(h)$ taken for the fluid layer to reduce to a thickness h:

$$t(h) = \frac{3\pi}{2L_0}\int_h^d \frac{\alpha s + k^{1/2}}{s^2(\alpha s^2 + 4k^{1/2}s + 6\delta\alpha k) + 12k(\alpha s + k^{1/2})}\,\mathrm{d}s. \tag{3.8}$$

In the special case in which the bed is impermeable, i.e. when $k = 0$, the fluid layer thickness $h = h(t)$ is given explicitly by

$$h = \left(\frac{3\pi d^2}{3\pi + 4d^2 L_0 t}\right)^{1/2}, \tag{3.9}$$

so that

$$h \sim \left(\frac{3\pi}{4L_0 t}\right)^{1/2} \to 0^+ \quad \text{as} \quad t \to \infty, \tag{3.10}$$

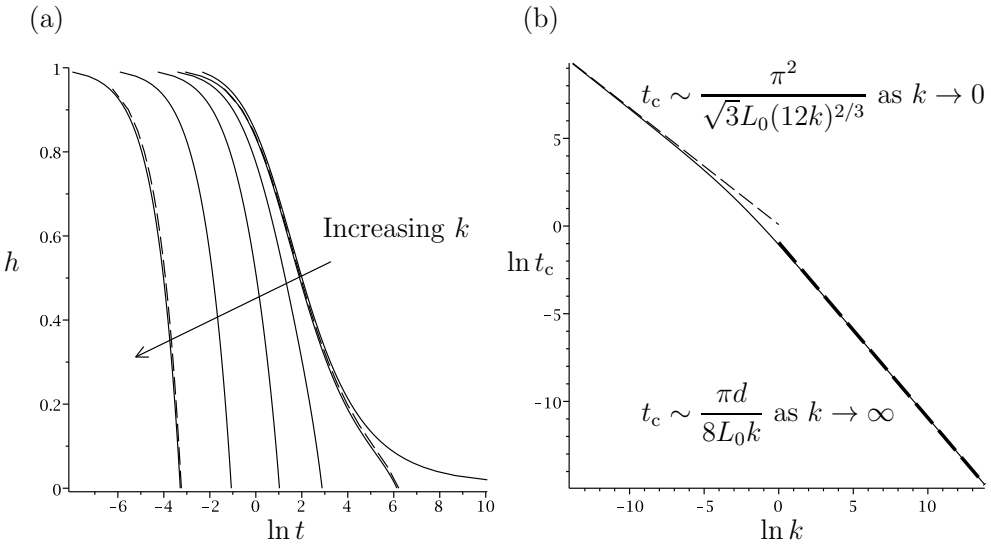

FIG. 3.1. *(a) Plots of the fluid layer thickness h as a function of $\ln t$ given by (3.8) for $k = 0$, 10^{-4}, 10^{-2}, 10^{-1}, 1 and 10 (solid lines), the uniformly valid leading order small-k asymptotic solution (4.33) for $k = 10^{-4}$ (dashed line) and the leading order large-k asymptotic solution (5.7) for $k = 10$ (dashed line). (b) Plots of $\ln t_c$ as a function of $\ln k$ given by (3.11) (solid line), the leading order small-k asymptotic solution (4.32) (dashed line) and the leading order large-k asymptotic solution (5.9) (bold dashed line). In all of the plots $\alpha = 1$*

i.e. an infinite time is required to squeeze all of the fluid out of the fluid layer (see, for example, Stone [26]).

In the general case $k \neq 0$ the integral in (3.8) was evaluated numerically using the `int` tool (with its default numerical method) in the computer algebra and numerical analysis package MAPLE. (Note that the integral in (3.8) may, in principal, be evaluated analytically, though this involves the zeros of the quartic expression appearing in the denominator of the integrand. These zeros may, in principal, be found using standard formulae; however, in practice, they are very unwieldy and so we always evaluated the integral numerically.)

Figure 3.1(a) shows plots of h as a function of $\ln t$ for different values of the permeability k. Figure 3.1(a) shows that, as expected, increasing k decreases the time taken for the fluid layer to reduce to a thickness h. Figure 3.1(a) also shows that when the bed is permeable, i.e. when $k \neq 0$, the bearing always makes contact with the porous bed in a finite time. This finite contact time is denoted by t_c, and is given by setting $h = 0$ in (3.8) to yield

$$t_c = \frac{3\pi}{2L_0} \int_0^d \frac{\alpha s + k^{1/2}}{s^2(\alpha s^2 + 4k^{1/2}s + 6\delta\alpha k) + 12k(\alpha s + k^{1/2})}\, \mathrm{d}s. \tag{3.11}$$

Figure 3.1(b) shows a plot of $\ln t_c$ as a function of $\ln k$. Figure 3.1(b) shows that, in agreement with Figure 3.1(a), increasing k decreases the contact time t_c. (In fact, it will be shown in §4.1 that $t_c = O(k^{-2/3}) \gg 1$ in the limit $k \to 0$ and in §5.1 that $t_c = O(k^{-1}) \ll 1$ in the limit $k \to \infty$.)

While the effect of varying the permeability k is relatively straightforward to understand, the effect of varying the Beavers–Joseph constant α is more subtle. Figure 3.2 shows plots of h as a function of t for different values of α for two values of k. In particular, Figure 3.2(a) shows that for a "small" value of k (specifically $k = 10^{-2}$) as α increases the time taken for the fluid layer to reduce to a thickness h increases,

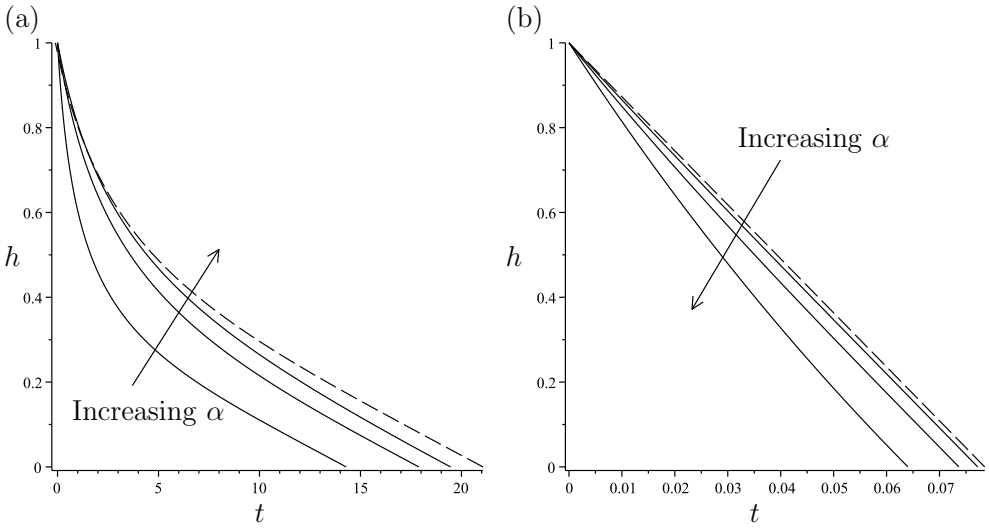

FIG. 3.2. *(a) Plots of the fluid layer thickness h as a function of t given by (3.8) for $\alpha = 10^{-2}$, $\alpha = 1$ and $\alpha = 100$ with $k = 10^{-2}$ (solid lines) and the uniformly valid leading order small-k asymptotic solution (4.33) with $k = 10^{-2}$ (dashed line). (b) Plots of h as a function of t given by (3.8) for $\alpha = 10^{-2}$, $\alpha = 1$ and $\alpha = 100$ with $k = 5$ (solid lines) and the leading order large-k asymptotic solution (5.7) with $k = 5$ (dashed line)*

whereas Figure 3.2(b) shows that for a "large" value of k (specifically $k = 5$) as α increases the time taken for the fluid layer to reduce to a thickness h decreases. This qualitative change in behaviour is confirmed by the analysis of the asymptotic limits $k \to 0$ and $k \to \infty$ given subsequently in §4 and §5, respectively.

To understand the physical reason why varying the Beavers–Joseph constant α has a qualitatively different effect for small and large values of the permeability k it is instructive to examine the radial fluid velocity v_r and the radial Darcy velocity u_r. Figure 3.3 shows plots of v_r as a function of z for $0 \leq z \leq h$ and of u_r as a function of z for $-1 \leq z \leq 0$ for different values of α for three values of the permeability k. (Note that all of the plots shown in Figure 3.3, and also all of those shown subsequently in Figure 3.4, are for the same value of the fluid layer thickness, namely $h = 1/2$, and so are therefore not at the same instant t.) Figure 3.3(a) shows the flow in the special case in which the bed is impermeable, i.e. when $k = 0$ and hence $l_{\rm s} = 0$, in which case there is, of course, no flow in the porous bed and no-slip between the fluid and the porous bed at the interface $z = 0$. Figures 3.3(b) and 3.3(c) show the flow for different values of α for a "small" (specifically $k = 10^{-2}$) and a "large" (specifically $k = 10$) value of the permeability k, respectively. Note that, since u_r is independent of both α and z, there is only a single uniform velocity profile in the porous bed in Figures 3.3(b) and 3.3(c). These figures also clearly show the effect of velocity slip at the interface $z = 0$, and that the fastest flow is in the fluid layer for small k but in the porous bed for large k. In particular, Figure 3.3(b) shows that when k is small increasing α (i.e. decreasing the slip length $l_{\rm s}$) decreases v_r and hence decreases the fluid volume flux out of the fluid layer into the region beyond $r = 1$, denoted by $Q_{\rm out}$ and given by

$$Q_{\rm out} = 2\pi \int_0^h v_r\, r|_{r=1}\, {\rm d}z = \frac{2L_0 h^2(\alpha h^2 + 4k^{1/2}h + 6\delta\alpha k)}{3(\alpha h + k^{1/2})}. \tag{3.12}$$

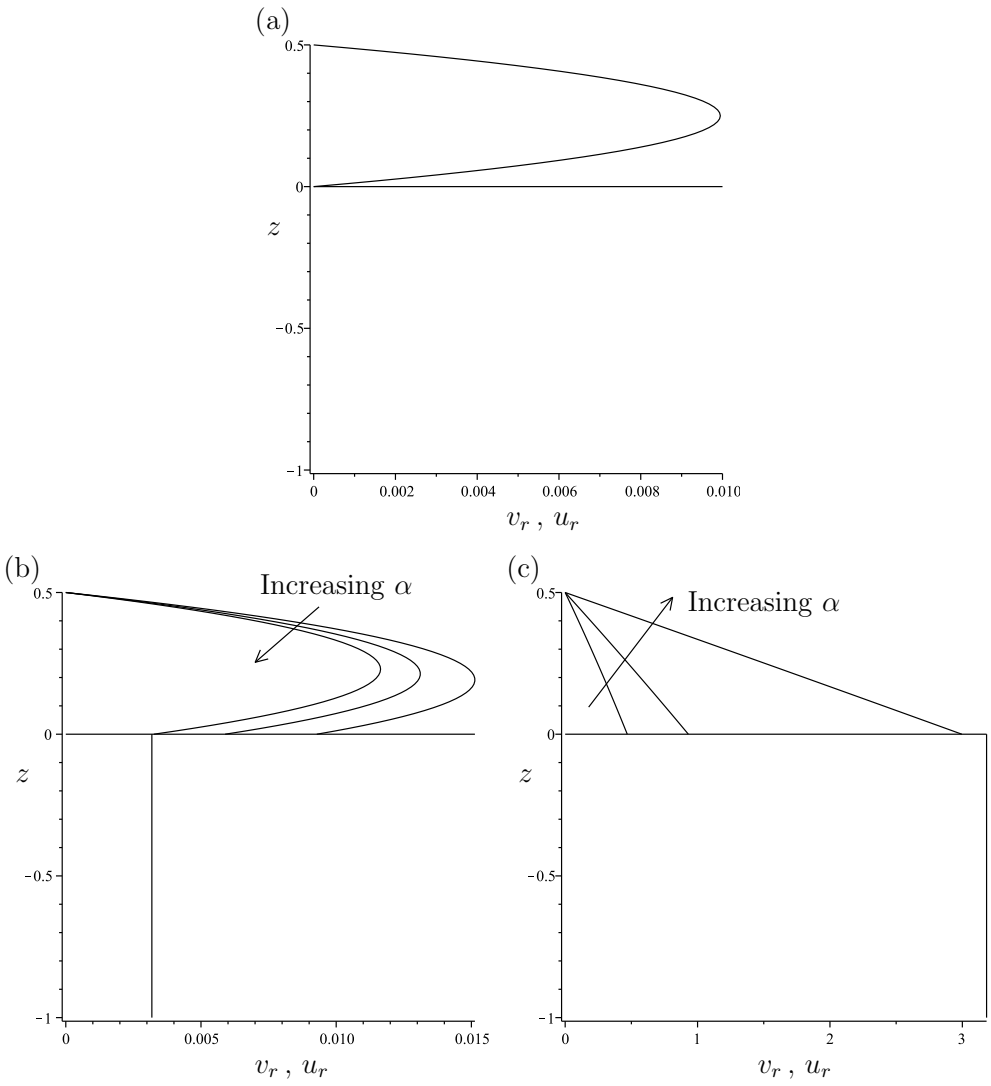

FIG. 3.3. *Plots of the radial fluid velocity v_r as a function of z for $0 \le z \le h$ and of the radial Darcy velocity u_r as a function of z for $-1 \le z \le 0$ at $r = 1/4$ when $h = 1/2$ for $\alpha = 1$, 2.5 and 100 with (a) $k = 0$, (b) $k = 10^{-2}$ and (c) $k = 10$*

Since the fluid volume flux into the porous bed, denoted by Q_{bed} and given by

$$Q_{\text{bed}} = 2\pi \int_0^1 v_z\, r|_{z=0}\, \mathrm{d}r = -8L_0 k, \tag{3.13}$$

is constant and independent of α, this decrease in Q_{out} causes the time taken for the fluid layer to reduce to a thickness h to increase, consistent with the behaviour for small k shown in Figure 3.2(a). On the other hand, Figure 3.3(c) shows that when k is large increasing α (i.e. decreasing the slip length l_{s}) increases v_r and hence increases Q_{out}, causing the time taken for the fluid layer to reduce to a thickness h to decrease, consistent with the behaviour for large k shown in Figure 3.2(b).

3.3. Instantaneous Streamlines. Figure 3.4 shows plots of the instantaneous streamlines for three values of the permeability k. Figure 3.4(a) shows the streamlines in the special case in which the bed is impermeable, i.e. when $k = 0$, in which case

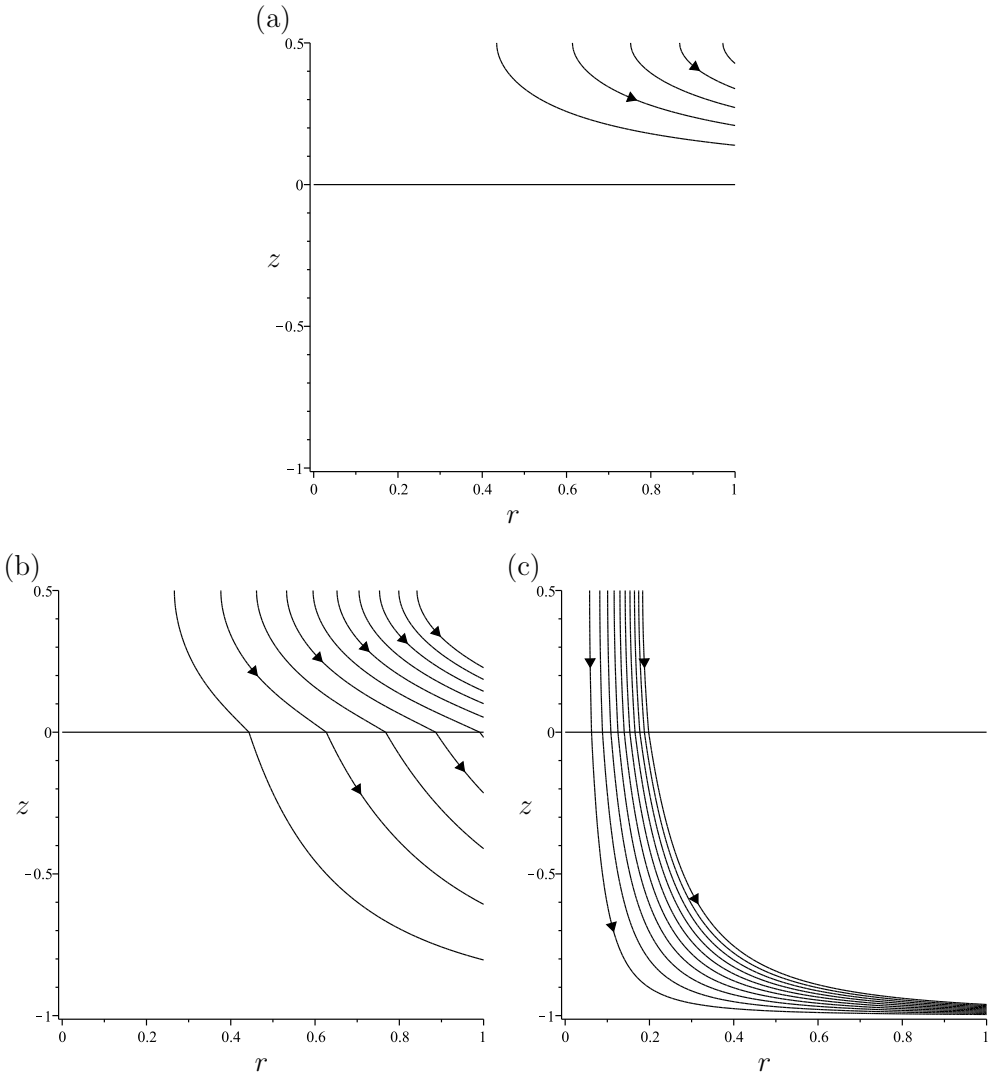

FIG. 3.4. *Plots of the instantaneous streamlines* $\psi = \text{constant} = -j/4 \times 10^{-2}$ *for* $j = 1, 2, \ldots, 10$ *with* ψ *given by (2.43) for* $0 \le z \le h$ *and (2.44) for* $-1 \le z < 0$ *when* $h = 1/2$ *for (a)* $k = 0$*, (b)* $k = 10^{-2}$ *and (c)* $k = 1/2$*. In all of the plots* $\alpha = 1$

there is, of course, no flow in the porous bed. Figures 3.4(b) and 3.4(c) show the streamlines for two non-zero values of the permeability k. In particular, they show that when the bed is permeable the vertical fluid velocity v_z on the interface $z = 0$ (which is given by $v_z|_{z=0} = u_z|_{z=0} = -8L_0k/\pi$) is always negative, and hence that fluid always flows from the fluid layer into the porous bed and never flows the other way. They also show that as k increases so do Q_{out} and Q_{bed}, and hence that the contact time t_{c} decreases, consistent with the behaviour shown in Figure 3.1.

3.4. Fluid Particle Paths and Penetration Depths. Using (3.2) to eliminate t from (2.45) and (2.46), the differential equations that govern the path (r, z) taken by a fluid particle are

$$(3.14)\quad \frac{1}{r}\frac{\mathrm{d}r}{\mathrm{d}h} = -\frac{3(h-z)\left[(\alpha h + k^{1/2})z + k^{1/2}(h + 2\delta\alpha k^{1/2})\right]}{h^2(\alpha h^2 + 4k^{1/2}h + 6\delta\alpha k) + 12k(\alpha h + k^{1/2})},$$

$$\frac{\mathrm{d}z}{\mathrm{d}h} = \frac{2(\alpha h + k^{1/2})(6k - z^3) + 3\alpha(h^2 - 2\delta k)z^2 + 6k^{1/2}h(h + 2\delta\alpha k^{1/2})z}{h^2(\alpha h^2 + 4k^{1/2}h + 6\delta\alpha k) + 12k(\alpha h + k^{1/2})} \tag{3.15}$$

in the fluid layer $0 \le z \le h$, and

$$\frac{1}{r}\frac{\mathrm{d}r}{\mathrm{d}h} = -\frac{6k(\alpha h + k^{1/2})}{\phi\left[h^2(\alpha h^2 + 4k^{1/2}h + 6\delta\alpha k) + 12k(\alpha h + k^{1/2})\right]}, \tag{3.16}$$

$$\frac{1}{1+z}\frac{\mathrm{d}z}{\mathrm{d}h} = \frac{12k(\alpha h + k^{1/2})}{\phi\left[h^2(\alpha h^2 + 4k^{1/2}h + 6\delta\alpha k) + 12k(\alpha h + k^{1/2})\right]} \tag{3.17}$$

in the porous bed $-1 \le z \le 0$, subject to the initial conditions

$$r = r_0 \quad \text{and} \quad z = z_0 \quad \text{when} \quad t = 0, \quad \text{i.e.} \quad \text{when} \quad h = d. \tag{3.18}$$

Integrating (3.16) and (3.17) subject to (3.18) shows that the particle paths in the porous bed are given by

$$\left(\frac{r}{r_0}\right)^2 = \frac{1+z_0}{1+z} = \exp\left[-\frac{12k}{\phi}\int_d^h \frac{\alpha s + k^{1/2}}{s^2(\alpha s^2 + 4k^{1/2}s + 6\delta\alpha k) + 12k(\alpha s + k^{1/2})}\,\mathrm{d}s\right], \tag{3.19}$$

and so, in particular, always satisfy $r^2(1+z) = r_0^2(1+z_0) = \text{constant}$.

Figure 3.5 shows the paths (r, z) taken by several fluid particles from their initial positions (r_0, z_0) at $t = 0$ for three values of the permeability k.

In the special case in which the bed is impermeable, i.e. when $k = 0$, equations (3.14) and (3.15) may be solved exactly subject to (3.18) to yield

$$r = r_0\left(\frac{4d(d - z_0)z_0 + (d - 2z_0)^2 h}{d^2 h}\right)^{3/4}, \tag{3.20}$$

$$z = \frac{h}{2}\left[1 - (d - 2z_0)\left(\frac{h}{4d(d - z_0)z_0 + (d - 2z_0)^2 h}\right)^{1/2}\right] \tag{3.21}$$

for $z_0 \ge 0$. Figure 3.5(a) shows the paths of several fluid particles in this case and, in particular, shows how all of the fluid particles eventually flow out of the fluid layer into the region beyond $r = 1$.

In the general case $k \ne 0$ the differential equations (3.14)–(3.17) were solved numerically using the `dsolve` tool (with its default numerical method) in MAPLE subject to (3.18). Figures 3.5(b) and 3.5(c) show the paths of several fluid particles for two non-zero values of the permeability k. In particular, they show that fluid particles initially in the fluid layer can either flow out of the fluid layer into the region beyond $r = 1$ or flow into the porous bed and then, in some cases, out of the porous bed into the region beyond $r = 1$. Since the vertical Darcy velocity $u_z = -8L_0k(1+z)/\pi$ is less than or equal to zero, fluid particles that enter the porous bed never re-enter the fluid layer, and fluid particles that are initially in the porous bed never enter the fluid layer. Figures 3.5(b) and 3.5(c) also show that as k increases then v_z increases relative to v_r so that the flow in the fluid layer is increasingly directed towards the porous bed, and consequently the fraction of the fluid particles initially in the fluid layer that flow into the porous bed increases.

Fluid particles initially in the fluid layer that enter the porous bed do so by crossing the interface $z = 0$ at some point $(r^*, 0)$, where $r^* = r^*(r_0, z_0)$, at $t = t^*$ corresponding to $h = h(t^*) = h^*$, and so the critical curve that divides the region of particles that enter the porous bed (with $r^* < 1$) from the region of those that do not

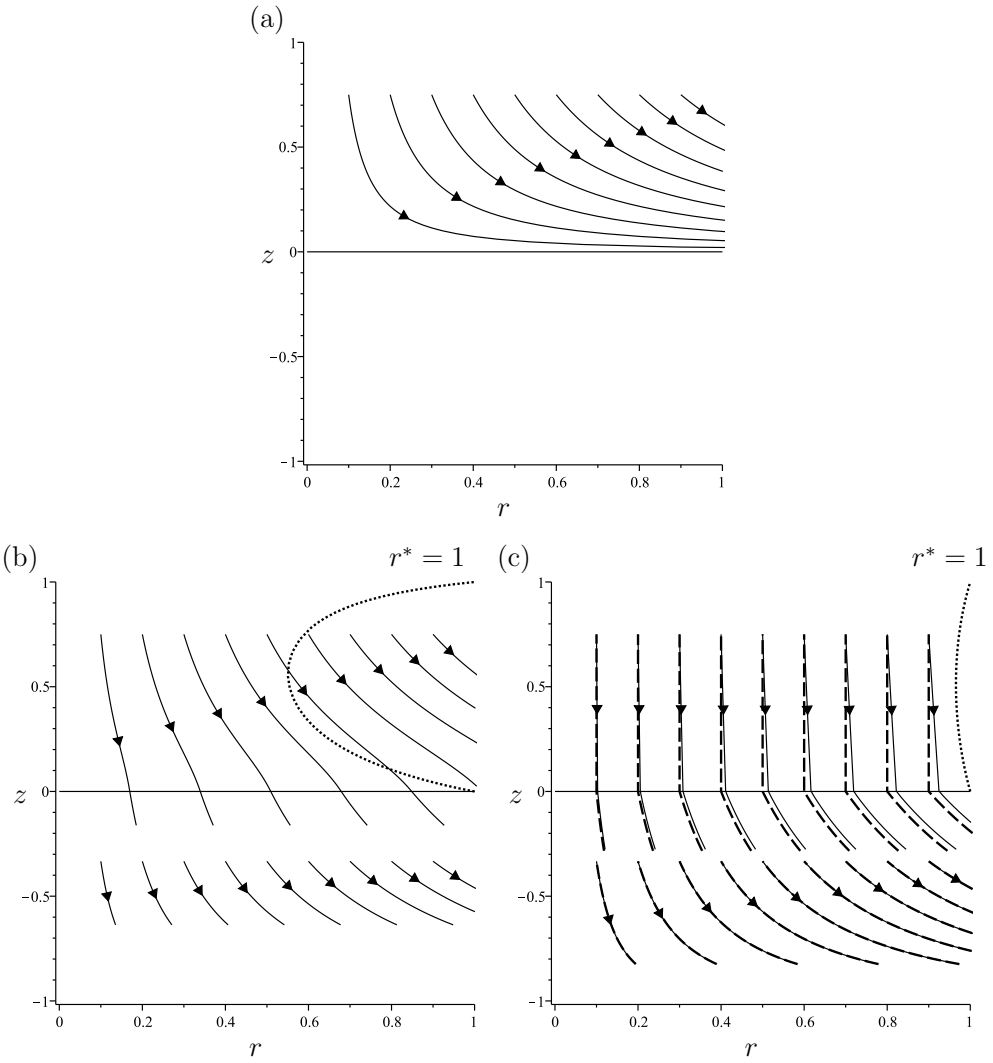

FIG. 3.5. *Plots of fluid particle paths* (r, z) *with* r *and* z *given by (a) (3.20) and (3.21) for* $(r_0, z_0) = (0.1, 0.75)$, $(0.2, 0.75)$, ..., $(0.9, 0.75)$, *(b,c) (3.14)–(3.17) subject to* $(r_0, z_0) = (0.1, 0.75)$, $(0.2, 0.75)$, ..., $(0.9, 0.75)$ *and* $(r_0, z_0) = (0.1, -1/3)$, $(0.2, -1/3)$, ..., $(0.9, -1/3)$ *for (b)* $k = 10^{-2}$ *and (c)* $k = 10$ *(solid lines) and the leading order large-k asymptotic solutions (5.12), (5.16), (5.17), (5.19) and (5.20) (dashed lines) for* $\alpha = 1$ *and* $\phi = 3/4$. *Parts (b) and (c) also include plots of the curve* $r^* = 1$ *(dotted lines)*

is given by $r^* = 1$. The curve $r^* = 1$ is found by solving (3.14) and (3.15) subject to $r = 1$ and $z = 0$ at $h = h^*$ backwards in time, i.e. from $h = h^*$ to $h = d$. Evaluating the solution for (r, z) when $h = d$ yields the initial position (r_0, z_0) of the fluid particle that passes through the point $(r, z) = (1, 0)$ when $h = h^*$. Repeating this procedure for $0 \leq h^* \leq d$ yields the curve $r^* = 1$. Figures 3.5(b) and 3.5(c) include plots of the curve $r^* = 1$ calculated in this way and confirm that fluid particles that initially lie to the left of $r^* = 1$ flow from the fluid layer into the porous bed, and the fluid particles that initially lie to the right of $r^* = 1$ flow out of the fluid layer into the region beyond $r = 1$. Figure 3.6 shows plots of the curve $r^* = 1$ for different values of the permeability k. In particular, Figure 3.6 shows that as k increases the curve $r^* = 1$ moves to the right, i.e. less fluid flows out of the fluid layer into the region

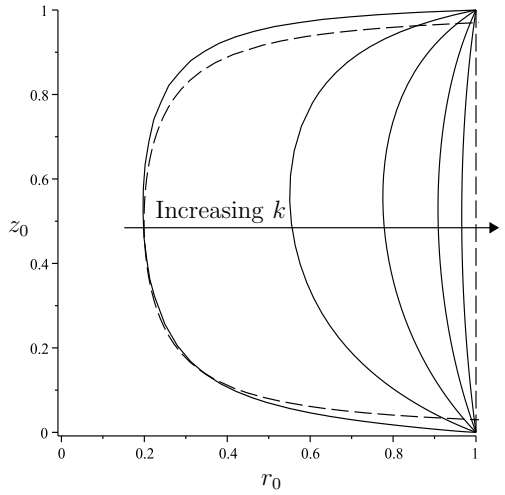

FIG. 3.6. *Plots of the critical curve $r^* = 1$ which divides the region of particles that enter the porous bed (with $r^* < 1$) from those that do not (with $r^* > 1$) for $k = 10^{-4}$, 10^{-2}, 10^{-1}, 1 and 10 (solid lines), the leading order small-k asymptotic solution (4.44) for $k = 10^{-4}$ (dashed line) and the leading order large-k asymptotic solution $r_0 = 1$ (dashed line). In all of the plots $\alpha = 1$*

beyond $r = 1$ and more fluid flows into the porous bed.

Also of considerable practical interest are the depths to which fluid particles (which may be initially situated in either the fluid layer or the porous bed) penetrate into the porous bed, denoted by $z_{\rm pen}$ and given by $z_{\rm pen} = z(t_{\rm c}) < 0$. Since both v_z and u_z are independent of r, $z_{\rm pen}$ is independent of r_0. However, the value of r_0 does affect whether or not a fluid particle flows into the region beyond $r = 1$. Figure 3.7(a) shows plots of $\ln|z_{\rm pen}|$ as a function of $\ln k$ for "small" values of the permeability k for three fluid particles initially situated in the fluid layer with $r_0 = O(k^{1/4})$. In particular, Figure 3.7(a) shows that $|z_{\rm pen}|$ decreases as k decreases and/or z_0 increases. Moreover, the effect of z_0 on $z_{\rm pen}$ becomes less pronounced as k decreases. (In fact, it will be shown in §4.2 that at leading order in the limit of small permeability $k \to 0$ the penetration depth $z_{\rm pen} = O(k^{1/3}) \ll 1$ of a fluid particle initially situated in the fluid layer with $r_0 = O(k^{1/4})$ is small and independent of z_0.) Figure 3.7(b) shows plots of $z_{\rm pen}$ as a function of $\ln k$ for "large" values of the permeability k for three fluid particles initially situated in the fluid layer. In particular, Figure 3.7(b) shows that again $|z_{\rm pen}|$ decreases as k decreases and/or z_0 increases. However, in this case, the effect of k on $z_{\rm pen}$ becomes less pronounced as k increases. (In fact, it will be shown in §5.2 that at leading order in the limit $k \to \infty$ the penetration depth $z_{\rm pen} = O(1)$ of a fluid particle initially situated in the fluid layer is independent of k and its magnitude decreases monotonically as z_0 increases.) Figure 3.7(c) shows plots of $\ln|z_{\rm pen} - z_0|$ as a function of $\ln k$ for "small" values of the permeability k for three fluid particles initially situated in the porous bed. In particular, Figure 3.7(c) shows that $|z_{\rm pen} - z_0|$ decreases as k decreases and/or z_0 decreases. (In fact, it will be shown in §4.2 that at leading order in the limit $k \to 0$ the magnitude of the relative penetration depth $|z_{\rm pen} - z_0| = O(k^{1/3}) \ll 1$ of a fluid particle initially situated in the porous bed is small and decreases monotonically as z_0 decreases.) Figure 3.7(d) shows plots of $z_{\rm pen}$ as a function of $\ln k$ for "large" values of the permeability k for three fluid particles initially situated in the porous bed. In particular, Figure 3.7(d) shows that, like in Figure 3.7(b), $|z_{\rm pen}|$ decreases as k decreases and/or z_0 increases. Moreover, the effect of k on $z_{\rm pen}$ becomes less pronounced as k increases. (In fact, it will be shown in §5.2 that at leading order in the limit of large permeability $k \to \infty$ the penetration depth

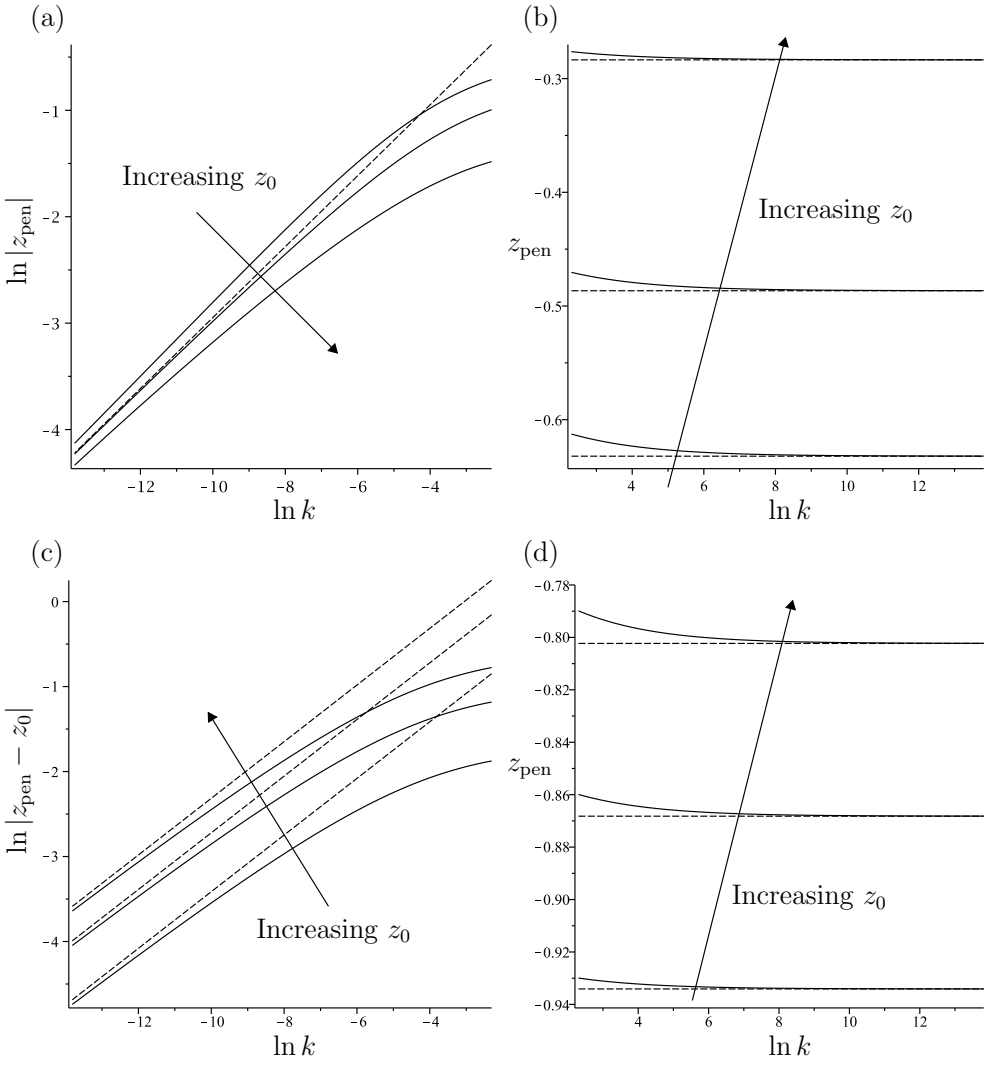

FIG. 3.7. *(a) Plots of* $\ln|z_{\rm pen}|$ *as a function of* $\ln k$ *given by (3.14)–(3.17) subject to* $(r_0, z_0) = (0.5 \times (12k)^{1/4}, 0.25)$, $(0.5 \times (12k)^{1/4}, 0.5)$ *and* $(0.5 \times (12k)^{1/4}, 0.75)$ *(solid lines) and the leading order small-k asymptotic solution given by (4.49) (dashed line). (b) Plots of* $z_{\rm pen}$ *as a function of* $\ln k$ *given by (3.14)–(3.17) subject to* $(r_0, z_0) = (0.5, 0.25)$, $(0.5, 0.5)$ *and* $(0.5, 0.75)$ *(solid lines) and the leading order large-k asymptotic solution given by (5.18) (dashed lines). (c) Plots of* $\ln|z_{\rm pen} - z_0|$ *as a function of* $\ln k$ *given by (3.16) and (3.17) subject to* $(r_0, z_0) = (0.5, -0.25), (0.5, -0.5)$ *and* $(0.5, -0.75)$ *(solid lines) and the leading order small-k asymptotic solution given by (4.54) (dashed lines). (d) Plots of* $z_{\rm pen}$ *as a function of* $\ln k$ *given by (3.16) and (3.17) subject to* $(r_0, z_0) = (0.5, -0.25), (0.5, -0.5)$ *and* $(0.5, -0.75)$ *(solid lines) and the leading order large-k asymptotic solution given by (5.21) (dashed lines). In all of the plots* $\alpha = 1$ *and* $\phi = 3/4$

$z_{\rm pen} = O(1)$ of a fluid particle initially situated in the porous bed is independent of k and its magnitude decreases monotonically as z_0 increases.)

As we have already seen, there is qualitatively different behaviour for small and large values of the permeability k, and so in §4 and §5 we investigate the asymptotic behaviour of the solution in the limits $k \to 0$ and $k \to \infty$, respectively, in detail.

4. Limit of Small Permeability $k \to 0$. In this section asymptotic solutions for the fluid layer thickness $h = h(t)$ (§4.1) and the fluid particle paths (r, z) (§4.2) in the limit of small permeability $k \to 0$ are obtained.

In this limit it will transpire that the contact time $t_c = O(k^{-2/3}) \gg 1$ is large, and a regular perturbation solution for $h = h(t)$ in powers of $k^{1/2} \ll 1$ turns out to be valid only for "short" times $t = O(1)$ (more precisely, for $t = o(k^{-1/2})$), and additional asymptotic solutions valid for "intermediate" times $t = O(k^{-1/2})$ and "long" times $t = O(k^{-2/3})$ are required in order to obtain a complete description of the behaviour up to the contact time.

4.1. Asymptotic Solution for $h = h(t)$.

4.1.1. Solution for "Short" Times $t = O(1)$. Seeking a regular perturbation solution to (3.2) with $L = L_0$ of the form

$$h(t) = h_0(t) + k^{1/2}h_1(t) + kh_2(t) + O(k^{3/2}), \tag{4.1}$$

at $O(1)$, $O(k^{1/2})$ and $O(k)$ we have

$$\frac{\mathrm{d}h_0}{\mathrm{d}t} = -\frac{2L_0h_0^3}{3\pi}, \tag{4.2}$$

$$\frac{\mathrm{d}h_1}{\mathrm{d}h_0} - \frac{3}{h_0}h_1 = \frac{3}{\alpha h_0}, \tag{4.3}$$

$$\frac{\mathrm{d}h_2}{\mathrm{d}h_0} - \frac{3}{h_0}h_2 = \frac{3\left[h_0(\alpha^2h_1^2 + 2\alpha h_1 + 2\delta\alpha^2 - 1) + 4\alpha^2\right]}{\alpha^2h_0^3}, \tag{4.4}$$

respectively, where t has been eliminated from (4.3) and (4.4) using (4.2). Solving (4.2)–(4.4) subject to the initial conditions $h_0(0) = d$, $h_1(0) = 0$ and $h_2(0) = 0$ yields the solutions

$$h_0 = \left(\frac{3\pi d^2}{3\pi + 4d^2L_0t}\right)^{1/2}, \tag{4.5}$$

$$h_1 = -\frac{(d^3 - {h_0}^3)}{\alpha d^3}, \tag{4.6}$$

$$h_2 = \frac{3\left[5{h_0}^7 + (5\delta\alpha^2d^2 + 8\alpha^2d - 10d^2){h_0}^5 + 5(1 - \delta\alpha^2)d^6h_0 - 8\alpha^2d^6\right]}{10\alpha^2d^6{h_0}^2}. \tag{4.7}$$

The leading order solution for h_0 given by (4.5) is simply the solution for an impermeable bed given by (3.9), i.e., as expected, the porous bed is effectively impermeable at leading order. The effect of permeability first appears at first order and, since h_1 given by (4.6) is negative for all $t > 0$, its effect is, as expected, to decrease the time t taken for the fluid layer to reduce to a thickness h. However, since

$$h_0 \sim \left(\frac{3\pi}{4L_0t}\right)^{1/2} \to 0^+, \quad h_1 \to -\frac{1}{\alpha}, \quad h_2 \sim -\frac{16L_0t}{5\pi} \to -\infty \quad \text{as} \quad t \to \infty, \tag{4.8}$$

the expansion (4.1) is not uniformly valid for all t. Comparing the leading and first order terms suggests that the expansion remains uniformly valid provided that

$$t \ll \frac{\alpha^2}{L_0k}, \quad \text{i.e.} \quad t = o(k^{-1}). \tag{4.9}$$

However, comparing the first and second order terms shows that in fact the expansion remains uniformly valid only provided that

$$t \ll \frac{1}{L_0 \alpha k^{1/2}}, \quad \text{i.e.} \quad t = o(k^{-1/2}), \tag{4.10}$$

and hence a second asymptotic solution valid for "intermediate" times $t = O(k^{-1/2})$ for which $h = O(k^{1/4})$ is necessary.

4.1.2. Solution for "Intermediate" Times $t = O(k^{-1/2})$. For "intermediate" times $t = O(k^{-1/2})$ we re-scale t and h according to

$$t = k^{-1/2}\hat{t}, \quad h = k^{1/4}\hat{h}, \tag{4.11}$$

where $\hat{t}$ and $\hat{h}$ are $O(1)$ in the limit $k \to 0$. Seeking a regular perturbation solution to (3.2) with $L = L_0$ of the form

$$\hat{h}(\hat{t}) = \hat{h}_0(\hat{t}) + k^{1/4}\hat{h}_1(\hat{t}) + O(k^{1/2}), \tag{4.12}$$

at $O(1)$ and $O(k^{1/4})$ we have

$$\frac{\mathrm{d}\hat{h}_0}{\mathrm{d}\hat{t}} = -\frac{2L_0\hat{h}_0^3}{3\pi}, \tag{4.13}$$

$$\frac{\mathrm{d}\hat{h}_1}{\mathrm{d}\hat{h}_0} - \frac{3}{\hat{h}_0}\hat{h}_1 = \frac{3(4\alpha + \hat{h}_0^2)}{\alpha\hat{h}_0^3}, \tag{4.14}$$

respectively. Solving (4.13) and (4.14) subject to the appropriate matching conditions with the solution at "short" times, namely

$$\hat{h}_0 \sim \left(\frac{3\pi}{4L_0\hat{t}}\right)^{1/2} \to \infty, \quad \hat{h}_1 \to -\frac{1}{\alpha} \quad \text{as} \quad \hat{t} \to 0, \tag{4.15}$$

yields the solutions

$$\hat{h}_0 = \left(\frac{3\pi}{4L_0\hat{t}}\right)^{1/2}, \tag{4.16}$$

$$\hat{h}_1 = -\frac{12\alpha + 5\hat{h}_0^2}{5\alpha\hat{h}_0^2}. \tag{4.17}$$

This solution for "intermediate" times is qualitatively similar to that for "short" times. However, since

$$\hat{h}_0 = \left(\frac{3\pi}{4L_0\hat{t}}\right)^{1/2} \to 0^+, \quad \hat{h}_1 \sim -\frac{16L_0\hat{t}}{5\pi} \to -\infty \quad \text{as} \quad \hat{t} \to \infty, \tag{4.18}$$

now the expansion remains uniformly valid provided that

$$\hat{t} \ll \frac{1}{L_0 k^{1/6}}, \quad \text{i.e.} \quad t \ll \frac{1}{L_0 k^{2/3}}, \tag{4.19}$$

and hence a third (and final) asymptotic solution valid for "long" times $t = O(k^{-2/3})$ for which $h = O(k^{1/3})$ is necessary.

4.1.3. Solution for "Long" Times $t = O(k^{-2/3})$. For "long" times $t = O(k^{-2/3})$ we re-scale t and h according to

$$t = (12k)^{-2/3}T, \quad h = (12k)^{1/3}H, \tag{4.20}$$

where T and H are $O(1)$ in the limit $k \to 0$ and the factor 12 has been introduced into the scalings for convenience. Seeking a regular perturbation solution to (3.2) with $L = L_0$ of the form

$$H(T) = H_0(T) + (12k)^{1/6}H_1(T) + O(k^{1/3}), \tag{4.21}$$

at $O(1)$ and $O(k^{1/6})$ we have

$$\frac{\mathrm{d}H_0}{\mathrm{d}T} = -\frac{2L_0(H_0^3+1)}{3\pi}, \tag{4.22}$$

$$\frac{\mathrm{d}H_1}{\mathrm{d}H_0} - \frac{3H_0^2}{H_0^3+1}H_1 = \frac{\sqrt{3}H_0^2}{2\alpha(H_0^3+1)}, \tag{4.23}$$

respectively. Solving (4.22) and (4.23) subject to the appropriate matching conditions with the solution at "intermediate" times, namely

$$H_0 \sim \left(\frac{3\pi}{4L_0T}\right)^{1/2} \to \infty, \quad H_1 \to -\frac{1}{2\sqrt{3}\alpha} \quad \text{as} \quad T \to 0, \tag{4.24}$$

yields the solutions

$$T = \frac{\pi[f(\infty) - f(H_0)]}{2L_0}, \tag{4.25}$$

$$H_1 = -\frac{1}{2\sqrt{3}\alpha}, \tag{4.26}$$

where the function $f = f(H_0)$ is given by

$$f(H_0) = \ln\left(\frac{H_0+1}{\sqrt{H_0^2 - H_0 + 1}}\right) + \sqrt{3}\tan^{-1}\left(\frac{2H_0-1}{\sqrt{3}}\right) \tag{4.27}$$

and satisfies $f(0) = -\sqrt{3}\pi/6$ and $f(\infty) = \sqrt{3}\pi/2$. Unlike for the solutions for "short" and "intermediate" times, the permeability now appears in the leading order solution and the solution remains uniformly valid up to the contact time $t = t_\mathrm{c}$ given by $t_\mathrm{c} = (12k)^{-2/3}T_\mathrm{c}$, where T_c satisfies $H(T_\mathrm{c}) = 0$, and has the asymptotic expansion

$$T_\mathrm{c} = T_{\mathrm{c}0} + (12k)^{1/6}T_{\mathrm{c}1} + O(k^{1/3}), \tag{4.28}$$

where

$$H_0(T_{\mathrm{c}0}) = 0, \quad T_{\mathrm{c}1} = -\frac{H_1(T_{\mathrm{c}0})}{H_0'(T_{\mathrm{c}0})}, \tag{4.29}$$

so that

$$T_{\mathrm{c}0} = \frac{\pi^2}{\sqrt{3}L_0}, \quad T_{\mathrm{c}1} = -\frac{\sqrt{3}\pi}{4L_0\alpha}. \tag{4.30}$$

Expressed in terms of the original variables the asymptotic expansion for the contact time (4.28) is therefore

$$t_c = \frac{\pi^2}{\sqrt{3}L_0(12k)^{2/3}} - \frac{\pi}{8L_0\alpha k^{1/2}} + O(k^{-1/3}). \tag{4.31}$$

In particular, the leading order small-k solution for the contact time given by

$$t_c = \frac{\pi^2}{\sqrt{3}L_0(12k)^{2/3}} \tag{4.32}$$

is independent of both α and δ, and so is the same for all three choices of boundary condition (2.9)–(2.11). Figure 3.1(b) compares the leading order small-k asymptotic solution for t_c given by (4.32) with the exact solution given by (3.11). The Beavers–Joseph constant α appears at first order in the asymptotic expansion for t_c given by (4.31), and inspection of the first order term reveals that decreasing α (i.e. increasing the slip length l_s) decreases the contact time t_c, consistent with the behaviour shown in Figure 3.2(a).

4.1.4. A Uniformly Valid Leading Order Composite Solution for $t(h)$. A uniformly valid leading order composite solution for $t = t(h)$ is

$$t(h) = -\frac{3\pi}{4d^2L_0} + (12k)^{-2/3}T\left(\frac{h}{(12k)^{1/3}}\right), \tag{4.33}$$

where T is given by (4.25). Figures 3.1(a) and 3.2(a) compare the uniformly valid leading order small-k asymptotic solution for $t = t(h)$ given by (4.33) with the exact solution for $t = t(h)$ given by (3.8). (Note that setting $h = d$ in (4.33) yields $t(d) = O(k)$ as $k \to 0$, so that (4.33) satisfies the initial condition (2.33) at leading order in the limit $k \to 0$. Similarly, setting $h = 0$ in (4.33) yields $t(0) \sim \pi^2/\sqrt{3}L_0(12k)^{2/3}$ as $k \to 0$, so that (4.33) coincides with (4.32) at leading order in the limit $k \to 0$.)

4.2. Asymptotic Solution for the Fluid Particle Paths.

4.2.1. Fluid Particles Initially Situated in the Fluid Layer $z_0 > 0$. The analysis in §4.1 shows that in the limit of small permeability $k \to 0$ the porous bed is effectively impermeable for "short" and "intermediate" times, i.e. for $t = o(k^{-2/3})$, and so at leading order the paths of fluid particles initially situated in the fluid layer (i.e. with $z_0 > 0$) are given by the solution for an impermeable bed given by (3.20) and (3.21). When $t = O(k^{-2/3})$ and $h = O(k^{1/3})$ the solution for an impermeable bed yields

$$r \sim r_0\left(\frac{4(d-z_0)z_0}{dh}\right)^{3/4} = O\left(\frac{r_0((d-z_0)z_0)^{3/4}}{k^{1/4}}\right), \tag{4.34}$$

$$z \sim \frac{h}{2} = O(k^{1/3}), \tag{4.35}$$

showing that only those fluid particles whose initial positions are close to the axis $r = 0$ (specifically, those with $r_0 = O(k^{1/4})$) or are close to either the porous bed or the bearing (specifically, those with $z_0 = O(k^{1/3})$ or $d - z_0 = O(k^{1/3})$, respectively) have not flowed out of the fluid layer into the region beyond $r = 1$ at "long" times.

In order to analyse the path of a fluid particle initially situated in the fluid layer close to the axis $r = 0$ with $r_0 = O(k^{1/4})$ and $z_0 > 0$ when $t = O(k^{-2/3})$ and $h = O(k^{1/3})$, we re-scale r_0, z, t and h according to

$$r_0 = (12k)^{1/4}R_0, \quad z = (12k)^{1/3}Z, \quad t = (12k)^{-2/3}T, \quad h = (12k)^{1/3}H, \tag{4.36}$$

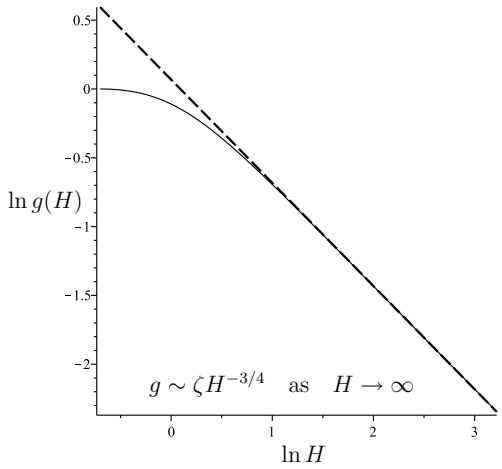

FIG. 4.1. *Plots of* $\ln g(H)$ *as a function of* $\ln H$ *given by (4.42) (solid line) and its large-H asymptotic behaviour* $g \sim \zeta H^{-3/4}$ *where* $\zeta \simeq 1.0708$ *(dashed line)*

where R_0, Z, T and H are $O(1)$ in the limit $k \to 0$ and the factor 12 has again been introduced into the scalings for convenience.

From (3.14) and (3.15) the leading order equations for the path of a fluid particle in the fluid layer are

$$\frac{1}{r}\frac{\mathrm{d}r}{\mathrm{d}H} = -\frac{3(H-Z)Z}{H^3+1}, \tag{4.37}$$

$$\frac{\mathrm{d}Z}{\mathrm{d}H} = \frac{-2Z^3+3HZ^2+1}{H^3+1}. \tag{4.38}$$

The solutions to (4.37) and (4.38) must match with the $h \to 0$ limits of (3.20) and (3.21) as $H \to \infty$, namely

$$r \sim R_0\left(\frac{4(d-z_0)z_0}{dH}\right)^{3/4} \to 0 \quad \text{as} \quad H \to \infty, \tag{4.39}$$

$$Z \sim \frac{H}{2} \to \infty \quad \text{as} \quad H \to \infty. \tag{4.40}$$

The leading order vertical position of the fluid particle $Z(T)$, which is independent of the initial height of the fluid particle z_0, was obtained numerically by posing (4.38) as an initial value problem by shooting from the value $Z = 0$ at the unknown value of the fluid layer thickness $H = H^*$ at which the fluid particle crosses the interface $Z = 0$ to $Z = H_\infty/2$ at some large value $H = H_\infty \gg 1$ approximating the matching condition (4.40) to within a prescribed tolerance, namely 10^{-6}. This procedure yielded the solution $H^* \simeq 0.4958$ corresponding to $T = T^* = T(H^*)$, which from (4.20) and (4.25) corresponds to the time

$$t = t^* = (12k)^{-2/3}T(H^*) \simeq \frac{0.6540}{L_0 k^{2/3}}. \tag{4.41}$$

The leading order radial position of the fluid particle $R(T)$ is calculated by integrating (4.37) from $H = H^*$ to H to obtain $r = r^* g(H)$, where $r = r^*$ is again the radial position at which the fluid particle crosses the interface $Z = 0$ and the function $g = g(H)$ is defined by

$$g(H) = \exp\left[-3\int_{H^*}^{H} \frac{(s-Z)Z}{s^3+1}\,\mathrm{d}s\right]. \tag{4.42}$$

Figure 4.1 shows a plot of $\ln g(H)$ as a function of $\ln H$ together with its large-H asymptotic behaviour $g \sim \zeta H^{-3/4}$ where $\zeta \simeq 1.0708$ as $H \to \infty$. Imposing the matching condition (4.39) yields

$$r^* = \frac{R_0}{\zeta}\left(\frac{4(d-z_0)z_0}{d}\right)^{3/4}. \tag{4.43}$$

In particular, the leading order solution for the critical curve $r^* = 1$ is therefore given by

$$r_0 = \zeta\left(\frac{d}{4(d-z_0)z_0}\right)^{3/4}(12k)^{1/4}. \tag{4.44}$$

Figure 3.6 compares the leading order small-k asymptotic solution (4.44) with the exact solution for $r^* = 1$ for $k = 10^{-4}$. In particular, it shows that the asymptotic solution compares favourably with the exact solution when $z_0 = O(1)$. However, as Figure 3.6 also shows, the asymptotic solution fails for $z_0 = O(k^{1/3}) \ll 1$ and for $d - z_0 = O(k^{1/3}) \ll 1$, i.e. for fluid particles that are initially close to either the porous bed or the bearing; for brevity these cases are not considered further here.

From (3.16) and (3.17) the leading order equations for the path of a fluid particle after it has entered the porous bed at $r = r^*$ are

$$\frac{\mathrm{d}R}{\mathrm{d}H} = -\frac{r^*}{2\phi(H^3+1)}, \tag{4.45}$$

$$\frac{\mathrm{d}Z}{\mathrm{d}H} = \frac{1}{\phi(H^3+1)}, \tag{4.46}$$

where we have written $r = r^* + (12k)^{1/3}R$. Solving (4.45) and (4.46) subject to the initial conditions $R = 0$ and $Z = 0$ at $H = H^*$ yields

$$r = r^*\left(1 + \frac{[f(H^*) - f(H)](12k)^{1/3}}{6\phi}\right), \tag{4.47}$$

$$z = -\frac{[f(H^*) - f(H)](12k)^{1/3}}{3\phi} \tag{4.48}$$

for $0 \le H < H^*$, where the function $f = f(H)$ is given by (4.27) and satisfies $f(H^*) \simeq 0.5381$, showing that the fluid particle remains close to $r = r^*$ and $z = 0$. In particular, setting $H = 0$ in (4.48) shows that the leading order asymptotic solution for z_{pen} is

$$z_{\mathrm{pen}} = -\frac{[f(H^*) - f(0)](12k)^{1/3}}{3\phi} \simeq -\frac{1.1027k^{1/3}}{\phi}, \tag{4.49}$$

which depends on k but is independent of z_0. Figure 3.7(a) compares the leading order small-k asymptotic solution for z_{pen} given by (4.49) with the exact solution.

Figure 4.2 compares the scaled fluid particle paths in (a) the fluid layer and (b) the porous bed with the leading order small-k asymptotic solution given by $r = r^* g(H)$ and the numerical solution of (4.38) for $H \ge H^*$, and by (4.47) and (4.48) for $0 \le H < H^*$.

4.2.2. Fluid Particles Initially Situated in the Porous Bed $z_0 < 0$. As we have already seen, the analysis in §4.1 shows that in the limit of small permeability $k \to 0$ the porous bed is effectively impermeable for "short" and "intermediate" times,

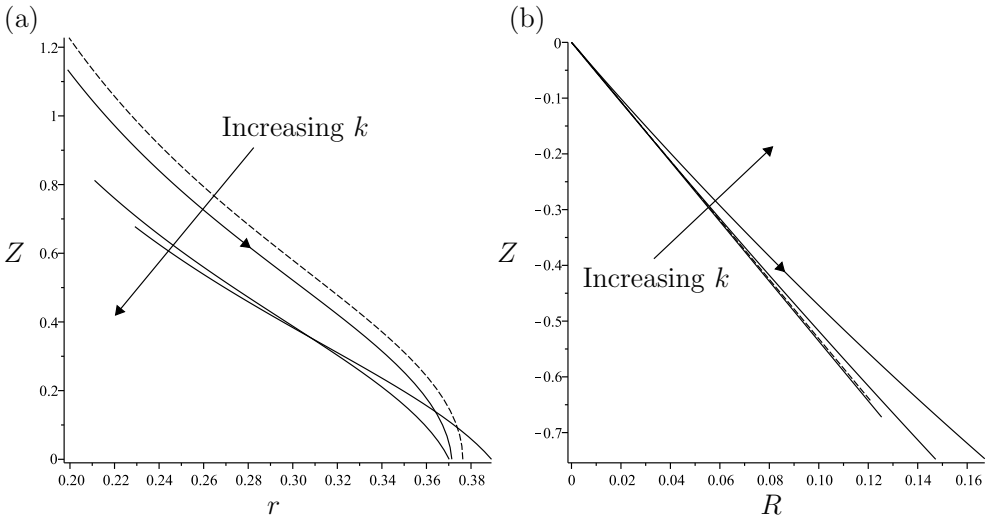

FIG. 4.2. *(a) Plots of the scaled fluid particle paths (r, Z) in the fluid layer where $Z = z/(12k)^{1/3}$ given by (3.14)–(3.17) subject to $(r_0, z_0) = (0.5\times(12k)^{1/4}, 0.25)$ for $k = 10^{-3}$, 10^{-4} and 10^{-8} (solid lines) and the leading order small-k asymptotic solution given by $r = r^*g(H)$ and the numerical solution of (4.38) for $H \geq H^*$ (dashed line). (b) Plots of the scaled fluid particle paths (R, Z) in the porous bed where $R = (r - r^*)/(12k)^{1/3}$ and $Z = z/(12k)^{1/3}$ given by (3.14)–(3.17) subject to $(r_0, z_0) = (0.5 \times (12k)^{1/4}, 0.25)$ for $k = 10^{-3}$, 10^{-4} and 10^{-8} and the leading order small-k asymptotic solution given by (4.47) and (4.48) for $0 \leq H < H^*$ (dashed line). In all of the plots $\alpha = 1$ and $\phi = 3/4$*

i.e. for $t = o(k^{-2/3})$, and so at leading order fluid particles initially situated in the porous bed (i.e. with $z_0 < 0$) remain close to their initial positions, specifically

$$r = r_0\left(1 + \frac{3(d^2 - h^2)k}{\phi d^2 h^2}\right), \tag{4.50}$$

$$z = z_0 - (1 + z_0)\frac{6(d^2 - h^2)k}{\phi d^2 h^2}. \tag{4.51}$$

For "long" times, i.e. for $t = O(k^{-2/3})$, a similar analysis to that described previously in §4.2.1 yields

$$r = r_0\left(1 + \frac{[f(\infty) - f(H)](12k)^{1/3}}{6\phi}\right), \tag{4.52}$$

$$z = z_0 - (1 + z_0)\frac{[f(\infty) - f(H)](12k)^{1/3}}{3\phi}, \tag{4.53}$$

$$z_{\rm pen} = z_0 - (1 + z_0)\frac{[f(\infty) - f(0)](12k)^{1/3}}{3\phi} = z_0 - \frac{2\pi(1 + z_0)(12k)^{1/3}}{3\sqrt{3}\phi}, \tag{4.54}$$

which depends on k and z_0. Figure 3.7(c) compares the leading order small-k asymptotic solution for $z_{\rm pen}$ given by (4.54) with the exact solution.

5. Limit of Large Permeability $k \to \infty$. In this section asymptotic solutions for the fluid layer thickness $h = h(t)$ (§5.1) and the fluid particle paths (r, z) (§5.2) in the limit of large permeability $k \to \infty$ are obtained.

In this limit it will transpire that the contact time $t_{\rm c} = O(k^{-1}) \ll 1$ is small, and, unlike in the limit of small permeability $k \to 0$ described in §4, a regular perturbation expansion for $h(t)$ in powers of $k^{-1/2} \ll 1$ is uniformly valid up to the contact time, making this limit somewhat easier to analyse.

5.1. Asymptotic Solution for $h = h(t)$. Since the contact time $t_c = O(k^{-1})$ we re-scale time t according to

$$t = k^{-1}T, \tag{5.1}$$

where T is $O(1)$ in the limit $k \to \infty$. Seeking a regular perturbation solution to (3.2) with $L = L_0$ of the form

$$h(T) = h_0(T) + k^{-1/2}h_1(T) + O(k^{-1}), \tag{5.2}$$

at $O(1)$ and $O(k^{-1/2})$ we have

$$\frac{\mathrm{d}h_0}{\mathrm{d}T} = -\frac{8L_0}{\pi}, \tag{5.3}$$

$$\frac{\mathrm{d}h_1}{\mathrm{d}h_0} = \frac{\delta\alpha h_0^2}{2}, \tag{5.4}$$

respectively. Solving (5.3) and (5.4) subject to the initial conditions $h_0(0) = d$ and $h_1(0) = 0$ yields the solutions

$$h_0 = d - \frac{8L_0T}{\pi}, \tag{5.5}$$

$$h_1 = -\frac{\delta\alpha(d^3 - h_0^3)}{6}. \tag{5.6}$$

Note that, unlike in the limit of small permeability $k \to 0$, the effect of permeability appears at leading order and the leading order solution h_0 given by (5.5) becomes zero at the finite time $T = T_c = \pi d/8L_0$. Figures 3.1(a) and 3.2(b) compare the leading order large-k asymptotic solution for $h = h(t)$, i.e.

$$h = d - \frac{8L_0kt}{\pi}, \tag{5.7}$$

with the exact solution for $t = t(h)$ given by (3.8). The contact time $t = t_c$ has the asymptotic expansion

$$t_c = \frac{\pi d}{8L_0k} - \frac{\pi\delta\alpha d^3}{48L_0k^{3/2}} + O(k^{-2}). \tag{5.8}$$

Figure 3.1(b) compares the leading order large-k asymptotic solution for t_c, i.e.

$$t_c = \frac{\pi d}{8L_0k}, \tag{5.9}$$

with the exact solution given by (3.11). As for the corresponding result in the limit of small permeability $k \to 0$ given by (4.31), the Beavers–Joseph constant α appears at first order in the large-k asymptotic expansion for t_c given by (5.8), but inspection of the first order term reveals that increasing the slip length l_s now increases (rather than decreases) the contact time t_c, consistent with the behaviour shown in Figure 3.2(b). However, unlike in the limit of small permeability $k \to 0$, the asymptotic expansion for t_c given by (5.8) is not uniformly valid in the limit $\alpha \to \infty$ (i.e. in the special case of zero slip length, $l_s = 0$) corresponding to the boundary condition (2.10), and so this case is treated separately in Appendix B.

5.2. Asymptotic Solution for the Fluid Particle Paths.

5.2.1. Fluid Particles Initially Situated in the Fluid Layer $z_0 > 0$. From (3.14) and (3.15) the leading order equations for the path of a fluid particle in the fluid layer are simply

$$\frac{\mathrm{d}r}{\mathrm{d}h} = 0, \tag{5.10}$$

$$\frac{\mathrm{d}z}{\mathrm{d}h} = 1. \tag{5.11}$$

Solving (5.10) and (5.11) subject to (3.18) yields

$$r = r_0 \quad \text{and} \quad z = h - h^*, \tag{5.12}$$

where $h^* = d - z_0$, showing that (since $v_z = O(k) \gg 1$ is larger than $v_r = O(k^{1/2}) \gg 1$) at leading order the particle moves vertically downwards through the fluid layer, reaching the interface $z = 0$ when $h = h^*$ corresponding to $T = T^* = \pi z_0/8L_0$, which from (5.1) corresponds to the time

$$t = t^* = \frac{\pi z_0}{8L_0 k}. \tag{5.13}$$

In particular, this means that the leading order large-k asymptotic approximation to the curve $r^* = 1$ is simply the straight line $r_0 = 1$. Figure 3.6 compares the straight line $r_0 = 1$ with the exact solution for $r^* = 1$ for $k = 10$.

From (3.16) and (3.17) the leading order equations for the path of a fluid particle after it has entered the porous bed are

$$\frac{1}{r}\frac{\mathrm{d}r}{\mathrm{d}h} = -\frac{1}{2\phi}, \tag{5.14}$$

$$\frac{1}{1+z}\frac{\mathrm{d}z}{\mathrm{d}h} = \frac{1}{\phi}. \tag{5.15}$$

Solving (5.14) and (5.15) subject to the initial conditions $r = r_0$ and $z = 0$ at $h = h^*$ yields

$$r = r_0 \exp\left(\frac{h^* - h}{2\phi}\right), \tag{5.16}$$

$$z = -1 + \exp\left(-\frac{h^* - h}{\phi}\right) \tag{5.17}$$

for $0 \le h < h^*$. In particular, setting $h = 0$ in (5.17) shows that the leading order asymptotic solution for z_{pen} is

$$z_{\mathrm{pen}} = -1 + \exp\left(-\frac{h^*}{\phi}\right), \tag{5.18}$$

which, in contrast to the corresponding result in the limit of small permeability $k \to 0$ given by (4.49), depends on z_0 (via h^*) but is independent of k. Figure 3.5(c) compares the fluid particle paths (r, z) with the leading order large-k asymptotic solution given by (5.12), (5.16) and (5.17). Figure 3.7(b) compares the leading order large-k asymptotic solution for z_{pen} given by (5.18) with the exact solution.

Parameter	Typical Size	Units	Reference
μ	$O(10^{-2})$	Pa s	Stewart *et al.* [25]
$\mathcal{R}$	$O(10^{-2})$	m	Nuño and Ahmed [18]
L	$O(10^{3})$	N	Stewart *et al.* [25]
$H_{\rm p}$	$O(10^{-3})$	m	Ateshian and Hung [3]
k	$O(10^{-18})$	m^2	Ateshian and Hung [3]

TABLE 6.1

Typical sizes of the dimensional parameters appearing in the model relevant to the human knee joint

5.2.2. Fluid Particles Initially Situated in the Porous Bed $z_0 < 0$. A similar analysis for fluid particles initially situated in the porous bed (i.e. with $z_0 < 0$) yields

$$r = r_0 \exp\left(\frac{d-h}{2\phi}\right), \tag{5.19}$$

$$z = -1 + (1+z_0)\exp\left(-\frac{d-h}{\phi}\right), \tag{5.20}$$

$$z_{\rm pen} = -1 + (1+z_0)\exp\left(-\frac{d}{\phi}\right). \tag{5.21}$$

Figure 3.5(c) compares the fluid particle paths (r, z) with the leading order large-k asymptotic solution given by (5.19) and (5.20). Figure 3.7(d) compares the leading order large-k asymptotic solution for $z_{\rm pen}$ given by (5.21) with the exact solution.

6. Conclusions. Motivated by the desire for a better understanding of the lubrication of the human knee joint, in the present work we considered the squeeze-film flow of a thin layer of Newtonian fluid (representing the synovial fluid) filling the gap between a flat impermeable surface (representing the femoral condyles) and a flat thin porous bed (representing the articular cartilage) coating a stationary flat impermeable surface (representing the tibial plateau).

Though this simple mathematical model does not explicitly include the effect of cartilage elasticity, by modelling the femoral condyles as a flat surface we accounted for an anticipated effect of cartilage elasticity, namely the formation of a fluid layer of approximately uniform thickness.

It was shown that as the impermeable surface approaches the porous bed under a prescribed constant load all of the fluid is squeezed out of the gap in a finite contact time $t_{\rm c}$. This contact time increases as the permeability of the porous bed decreases, and satisfies $t_{\rm c} = O(k^{-2/3}) \gg 1$ in the limit of small permeability $k \to 0$ and $t_{\rm c} = O(k^{-1}) \ll 1$ in the limit of large permeability $k \to \infty$.

Typical sizes of the dimensional parameters appearing in the model relevant to the human knee joint are given in Table 6.1.[1] In particular, Table 6.1 shows that the non-dimensional permeability $k = O(10^{-12})$ is typically very small, meaning that the limit of small permeability $k \to 0$ is most relevant to the human knee. In this limit we found that the leading order asymptotic solution for $t_{\rm c}$ is given by (4.32), which is independent of the choice of boundary condition (2.9)–(2.11) and is expressed in

[1]Note that the porosity ϕ is not included in Table 6.1 as it is, by definition, dimensionless and $O(1)$. Ateshian and Hung [3] state that for the cartilage in an adult knee ϕ lies typically between 0.68 and 0.85.

terms of dimensional variables as

$$t_{\rm c} = \frac{\pi^2 \mu \mathcal{R}^4}{\sqrt{3} L (12 H_{\rm p} k)^{2/3}} = O(10)\,{\rm s}. \tag{6.1}$$

Hence the present model predicts that when a person stands still for a short period of time their knees may be fluid lubricated, but that when they stand still for a longer period of time contact between the cartilage-coated surfaces may occur. Of course, during physical activity such as walking or running a person repeatedly loads and unloads their knees with a temporally varying load. Since typically each step or stride takes around 1 s, which is somewhat less than the typical size of $t_{\rm c}$ given by (6.1), the present model also suggests that their knees may also remain fluid lubricated during walking or running. Moreover, the corresponding size of $h = O((H_{\rm p}k)^{1/3}) = O(10^{-7})$ m is consistent with the value of 5×10^{-7} m quoted by Stewart *et al.* [25].

We also found that in the limit of small permeability the leading order asymptotic solution for the penetration depth $z_{\rm pen}$ of fluid particles initially situated in the fluid layer into the porous bed is given by (4.49) and is expressed in terms of dimensional variables as

$$z_{\rm pen} = -\frac{1.1027 (H_{\rm p} k)^{1/3}}{\phi} = O(10^{-7})\,{\rm m}, \tag{6.2}$$

which is much less than $H_{\rm p}$. Hence the present model predicts that when a person stands still any nutrients initially in the fluid layer penetrate only a relatively small distance into the cartilage. Moreover, the relative penetration depth $z_{\rm pen} - z_0$ of fluid particles initially situated in the porous bed is given by (4.54) and is expressed in dimensional variables as

$$z_{\rm pen} - z_0 = -\frac{2\pi (H_{\rm p} + z_0)(12 H_{\rm p} k)^{1/3}}{3\sqrt{3}\phi H_{\rm p}} = O(10^{-7})\,{\rm m}, \tag{6.3}$$

which is of approximately the same size as $z_{\rm pen}$ given by (6.2). Hence the present model also predicts that when a person stands still any nutrients initially in the cartilage penetrate only a relatively small distance further into it. However, the cumulative effect of repeated loading and unloading of the knees may alter this conclusion. Assuming that a reasonably active person takes $O(10^4)$ steps per day, the size of the relative penetration depth given in (6.3) corresponds to a maximum cumulative vertical displacement of $O(10^{-3})$ m, which is comparable with $H_{\rm p}$, i.e. the present model also suggests that the cumulative effect of repeated loading and unloading of the knees during physical activity such as walking or running may be sufficient to carry nutrients deep into the cartilage.

Acknowledgements. All four authors gratefully acknowledge valuable discussions with Dr Richard Black, Dr Philip Riches and Mr Anthony Herbert from the Bioengineering Unit at the University of Strathclyde on the biomechanics of the knee.

Appendix A. Two-Dimensional Problem.

The main body of the present work concerns an axisymmetric problem which is most relevant to the human knee. However, the corresponding results for a two-dimensional bearing of semi-width $\mathcal{L}$ shown in Figure A.1 are also of interest, and may be obtained in a similar manner to those for the axisymmetric problem. In this Appendix the main results for the two-dimensional problem are described and the key similarities to and differences from the corresponding results for the axisymmetric problem are highlighted.

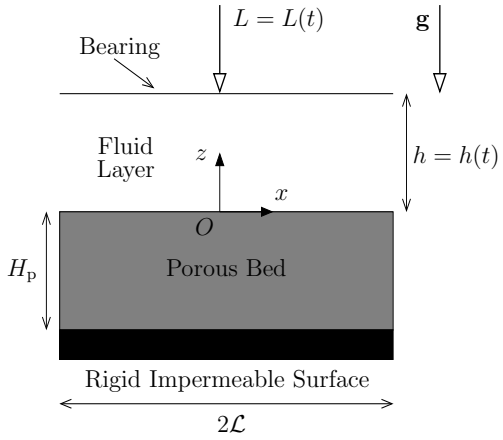

FIG. A.1. *The geometry of the two-dimensional problem*

Consider, with reference to the two-dimensional Cartesian coordinate system (x, z) shown in Figure A.1, the two-dimensional problem with (dimensional) load $L = L(t)$ per unit width. This problem is non-dimensionalised in the same way as the axisymmetric problem (2.16) with $\mathcal{L}$ in place of $\mathcal{R}$ and $\mu V\mathcal{L}^2/H_\mathrm{p}^2$ in place of $\mu V\mathcal{R}^3/H_\mathrm{p}^2$ as the characteristic scales for horizontal distance and load, respectively. The horizontal and vertical components of the fluid velocity, $v_x = v_x(x, z, t)$ and $v_z = v_z(x, z, t)$, are given by

$$v_x = -\frac{(h-z)\left[(\alpha h + k^{1/2})z + k^{1/2}(h + 2\delta\alpha k^{1/2})\right]}{2(\alpha h + k^{1/2})}\frac{\partial p}{\partial x}, \tag{A.1}$$

$$v_z = \frac{2(\alpha h + k^{1/2})(6k - z^3) + 3\alpha(h^2 - 2\delta k)z^2 + 6k^{1/2}h(h + 2\delta\alpha k^{1/2})z}{12(\alpha h + k^{1/2})}\frac{\partial^2 p}{\partial x^2}, \tag{A.2}$$

respectively, the horizontal and vertical components of the Darcy velocity, $u_x = u_x(x, z, t)$ and $u_z = u_z(x, z, t)$, are given by

$$u_x = -k\frac{\partial p}{\partial x}, \quad u_z = k(1+z)\frac{\partial^2 p}{\partial x^2}, \tag{A.3}$$

respectively, and the unsteady Reynolds equation governing the pressure $p = p(x, t)$ is

$$\frac{\mathrm{d}h}{\mathrm{d}t} = \frac{h^2(\alpha h^2 + 4k^{1/2}h + 6\delta\alpha k) + 12k(\alpha h + k^{1/2})}{12(\alpha h + k^{1/2})}\frac{\partial^2 p}{\partial x^2}. \tag{A.4}$$

Integrating (A.4) twice with respect to x, applying the boundary conditions $p = 0$ at $x = \pm 1$, and imposing the load condition

$$L(t) = 2\int_0^1 p\,\mathrm{d}x \tag{A.5}$$

yields the pressure

$$p = \frac{3L(t)(1 - x^2)}{4}, \tag{A.6}$$

and the differential equation governing the fluid layer thickness $h = h(t)$:

$$L(t) = -\frac{8(\alpha h + k^{1/2})}{h^2(\alpha h^2 + 4k^{1/2}h + 6\delta\alpha k) + 12k(\alpha h + k^{1/2})}\frac{\mathrm{d}h}{\mathrm{d}t}. \tag{A.7}$$

Equation (A.7) is very similar to the corresponding equation (3.2) in the axisymmetric case. In particular, in the special case of constant load $L = L_0 > 0$ equation (3.2) can be recovered from (A.7) simply by rescaling t with $3\pi t/16$, and hence the solutions for the fluid layer thickness $h = h(t)$ and the contact time t_c in the two-dimensional case may be readily obtained from the corresponding results in the axisymmetric case.

The path (x, z) taken by a fluid particle is governed by

$$\frac{1}{x}\frac{\mathrm{d}x}{\mathrm{d}h} = -\frac{6(h-z)\left[(\alpha h + k^{1/2})z + k^{1/2}(h + 2\delta\alpha k^{1/2})\right]}{h^2(\alpha h^2 + 4k^{1/2}h + 6\delta\alpha k) + 12k(\alpha h + k^{1/2})}, \tag{A.8}$$

$$\frac{\mathrm{d}z}{\mathrm{d}h} = \frac{2(\alpha h + k^{1/2})(6k - z^3) + 3\alpha(h^2 - 2\delta k)z^2 + 6k^{1/2}h(h + 2\delta\alpha k^{1/2})z}{h^2(\alpha h^2 + 4k^{1/2}h + 6\delta\alpha k) + 12k(\alpha h + k^{1/2})} \tag{A.9}$$

in the fluid layer $0 \le z \le h$, and

$$\frac{1}{x}\frac{\mathrm{d}x}{\mathrm{d}h} = -\frac{12k(\alpha h + k^{1/2})}{\phi\left[h^2(\alpha h^2 + 4k^{1/2}h + 6\delta\alpha k) + 12k(\alpha h + k^{1/2})\right]}, \tag{A.10}$$

$$\frac{1}{1+z}\frac{\mathrm{d}z}{\mathrm{d}h} = \frac{12k(\alpha h + k^{1/2})}{\phi\left[h^2(\alpha h^2 + 4k^{1/2}h + 6\delta\alpha k) + 12k(\alpha h + k^{1/2})\right]} \tag{A.11}$$

in the porous bed $-1 \le z \le 0$. Hence the particle paths in the porous bed are given by

$$\frac{x}{x_0} = \frac{1+z_0}{1+z} = \exp\left[-\frac{12k}{\phi}\int_d^h \frac{\alpha s + k^{1/2}}{s^2(\alpha s^2 + 4k^{1/2}s + 6\delta\alpha k) + 12k(\alpha s + k^{1/2})}\,\mathrm{d}s\right], \tag{A.12}$$

and so, in particular, always satisfy $x(1+z) = x_0(1+z_0) =$ constant. Equations (A.9) and (A.11), which govern the vertical position $z = z(t)$ of a fluid particle, are identical to the corresponding equations (3.15) and (3.17) in the axisymmetric case, and hence the solutions for $z = z(t)$ and z_{pen} in the two-dimensional case may be immediately obtained from the corresponding solutions in the axisymmetric case. Moreover, the right-hand sides of equations (A.8) and (A.10), which govern the horizontal position $x = x(t)$ of a fluid particle, differ from the right-hand sides of the corresponding equations (3.14) and (3.16) for $r = r(t)$ in the axisymmetric case by only a factor of 2, and so the solution for $x = x(t)$ in the two-dimensional case may be readily obtained from the solution for $r = r(t)$ in the axisymmetric case by using the simple relationship $x/x_0 = (r/r_0)^2$.

Appendix B. Limit of Large Permeability $k \to \infty$ in the Special Case of Zero Slip Length, $l_s = 0$.

As described in §5, in the limit of large permeability $k \to \infty$, the asymptotic expansion for the contact time t_c given by (5.8) is not uniformly valid in the limit $\alpha \to \infty$ (i.e. in the special case of zero slip length, $l_s = 0$) corresponding to the boundary condition (2.10), and so this case must be considered separately from the general analysis for finite α (i.e. for $l_s \neq 0$) described in the main body of the present work. Accordingly, in this Appendix asymptotic solutions for the fluid layer thickness $h = h(t)$ (§B.1) and the fluid particle paths (r, z) (§B.2) in the limit of large permeability $k \to \infty$ when $l_s = 0$ are obtained.

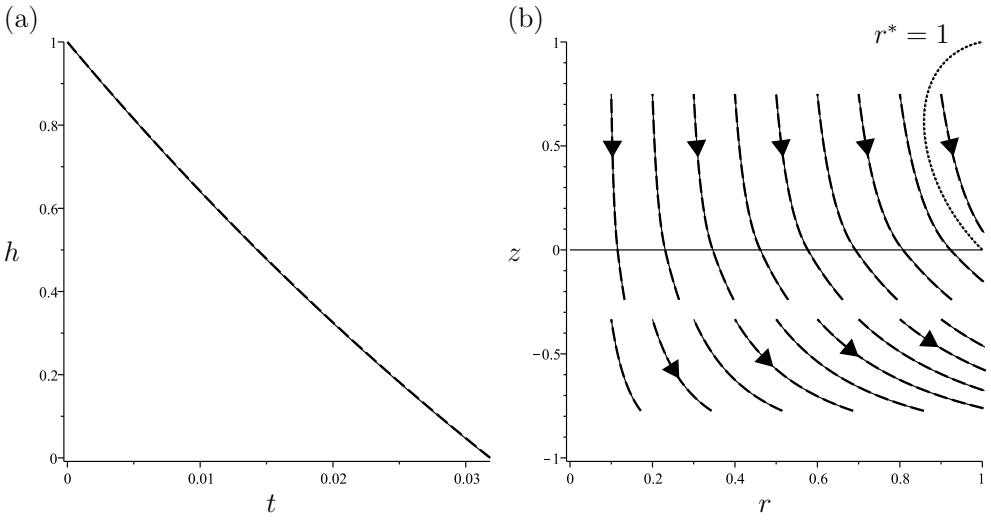

FIG. B.1. *(a) Plots of the fluid layer thickness h as a function of t in the case $l_s = 0$ given by (3.8) and the leading order large-k asymptotic solution (B.8) (dashed line) for $k = 10$. (b) Plots of fluid particle paths (r, z) in the case $l_s = 0$ where r and z are given by (B.2)–(B.5) subject to $(r_0, z_0) = (0.1, 0.75)$, $(0.2, 0.75)$, ..., $(0.9, 0.75)$ and $(r_0, z_0) = (0.1, -1/3)$, $(0.2, -1/3)$, ..., $(0.9, -1/3)$ (solid lines) and the leading order large-k asymptotic solutions (B.12), (B.13), (B.18), (B.19), (B.21) and (B.22) (dashed lines) for $k = 10$ and $\phi = 3/4$. Part (b) also includes a plot of the curve $r^* = 1$ (dotted line)*

When $l_s = 0$ the equation governing the fluid layer thickness $h = h(t)$ given by (3.2) with $L = L_0$ becomes

$$L_0 = -\frac{3\pi}{2\left[h^3 + 6k(h+2)\right]}\frac{\mathrm{d}h}{\mathrm{d}t}, \tag{B.1}$$

and the equations governing the fluid particle paths (r, z) given by (3.14)–(3.17) become

$$\frac{1}{r}\frac{\mathrm{d}r}{\mathrm{d}h} = -\frac{3(h-z)(hz+2k)}{h\left[h^3 + 6k(h+2)\right]}, \tag{B.2}$$

$$\frac{\mathrm{d}z}{\mathrm{d}h} = \frac{2h(6k - z^3) + 3(h^2 - 2k)z^2 + 12khz}{h\left[h^3 + 6k(h+2)\right]} \tag{B.3}$$

in the fluid layer $0 \le z \le h$, and

$$\frac{1}{r}\frac{\mathrm{d}r}{\mathrm{d}h} = -\frac{6k}{\phi\left[h^3 + 6k(h+2)\right]}, \tag{B.4}$$

$$\frac{1}{1+z}\frac{\mathrm{d}z}{\mathrm{d}h} = \frac{12k}{\phi\left[h^3 + 6k(h+2)\right]} \tag{B.5}$$

in the porous bed $-1 \le z \le 0$, respectively.

B.1. Asymptotic Solution for $h = h(t)$. At leading order in the limit of large permeability $k \to \infty$ equation (B.1) becomes

$$L_0 = -\frac{\pi}{4k(2+h)}\frac{\mathrm{d}h}{\mathrm{d}t}. \tag{B.6}$$

Solving (B.6) subject to the initial condition (2.33) yields

$$t = \frac{\pi}{4L_0 k}\ln\left(\frac{2+d}{2+h}\right), \tag{B.7}$$

which may be readily solved for h to obtain

$$h = -2 + (2+d)\exp\left(-\frac{4L_0kt}{\pi}\right). \tag{B.8}$$

Figure B.1(a) compares the leading order large-k asymptotic solution for $h = h(t)$ given by (B.8) with the exact solution for $t = t(h)$ given by (3.8) for $k = 10$. Setting $h = 0$ in (B.7) shows that the leading order large-k asymptotic solution for the contact time t_c is

$$t_c = \frac{\pi}{4L_0k}\ln\left(\frac{2+d}{2}\right). \tag{B.9}$$

Comparing (B.9) with the corresponding expression for the contact time t_c for a non-zero slip length $l_s \neq 0$ given by (5.9) shows that the latter is larger than the former by a factor of $d/2\ln(1+d/2) > 1$, meaning that, as expected, the effect of a non-zero slip length is to decrease Q_{out} and hence to increase the contact time t_c.

B.2. Asymptotic Solution for the Fluid Particle Paths.

B.2.1. Fluid Particles Initially Situated in the Fluid Layer $z_0 > 0$. At leading order equations (B.2) and (B.3) governing the path of a fluid particle through the fluid layer become

$$\frac{1}{r}\frac{\mathrm{d}r}{\mathrm{d}h} = -\frac{h-z}{h(2+h)}, \tag{B.10}$$

$$\frac{\mathrm{d}z}{\mathrm{d}h} = \frac{2h(1+z)-z^2}{h(2+h)}. \tag{B.11}$$

Solving (B.10) and (B.11) subject to (3.18) yields

$$r = r_0\left[1 - \frac{d-z_0}{2}\ln\left(\frac{(2+d)h}{d(2+h)}\right)\right], \tag{B.12}$$

$$z = h - \frac{d-z_0}{\left[1 - \frac{d-z_0}{2}\ln\left(\frac{(2+d)h}{d(2+h)}\right)\right]}, \tag{B.13}$$

which, in contrast to the corresponding results in the case of a non-zero slip length $l_s \neq 0$, show that (since both v_r and v_z are $O(k) \gg 1$) at leading order the particle moves both radially and vertically through the fluid layer. In particular, setting $z = 0$ in (B.13) shows that a fluid particle reaches the interface $z = 0$ when

$$h = h^* = -2\left[1 + W_{-1}\left(-\frac{2+d}{d}\exp\left(-\frac{2+d-z_0}{d-z_0}\right)\right)\right]^{-1}, \tag{B.14}$$

where W_{-1} denotes the lower real branch of the Lambert W function (see, for example, [30]), which, from (B.7), corresponds to the time

$$t = t^* = \frac{\pi}{4L_0k}\ln\left(\frac{2+d}{2+h^*}\right), \tag{B.15}$$

and, from (B.12), occurs at the radial position $r = r^*$, where $r^* = r_0(d-z_0)/h^*$. Hence at leading order the critical curve $r^* = 1$ is given by $r_0 = h^*/(d-z_0)$.

At leading order equations (B.4) and (B.5) governing the path of a fluid particle after it has entered the porous bed are

$$\frac{1}{r}\frac{\mathrm{d}r}{\mathrm{d}h} = -\frac{1}{\phi(2+h)}, \tag{B.16}$$

$$\frac{1}{1+z}\frac{\mathrm{d}z}{\mathrm{d}h} = \frac{2}{\phi(2+h)}. \tag{B.17}$$

Solving (B.16) and (B.17) subject to the initial conditions $r = r^*$ and $z = 0$ when $h = h^*$ yields

$$r = r^*\left(\frac{2+h^*}{2+h}\right)^{1/\phi}, \tag{B.18}$$

$$z = -1 + \left(\frac{2+h}{2+h^*}\right)^{2/\phi} \tag{B.19}$$

for $0 \le h < h^*$. In particular, setting $h = 0$ in (B.19) shows that the leading order asymptotic solution for z_{pen} is

$$z_{\mathrm{pen}} = -1 + \left(\frac{2}{2+h^*}\right)^{2/\phi}, \tag{B.20}$$

which, like the corresponding result in the case of a non-zero slip length $l_{\mathrm{s}} \neq 0$ given by (5.18), depends on z_0 (via h^*) but is independent of k. Figure B.1(b) compares the fluid particle paths (r, z) with the leading order large-k asymptotic solution given by (B.12), (B.13), (B.18) and (B.19).

B.2.2. Fluid Particles Initially Situated in the Porous Bed $z_0 < 0$. A similar analysis for fluid particles initially situated in the porous bed (i.e. with $z_0 < 0$) yields

$$r = r_0\left(\frac{2+d}{2+h}\right)^{1/\phi}, \tag{B.21}$$

$$z = -1 + (1+z_0)\left(\frac{2+h}{2+d}\right)^{2/\phi}, \tag{B.22}$$

$$z_{\mathrm{pen}} = -1 + (1+z_0)\left(\frac{2}{2+d}\right)^{2/\phi}. \tag{B.23}$$

Figure B.1(b) also compares the fluid particle paths (r, z) with the leading order large-k asymptotic solution given by (B.21) and (B.22).

REFERENCES

[1] D. J. Acheson, *Elementary Fluid Dynamics*, Oxford University Press (1990).

[2] N. Alleborn and H. Raszillier, *Spreading and sorption of a droplet on a porous substrate*, Chem. Eng. Sci., 59 (2004), pp. 2071–2088.

[3] G. A. Ateshian and C. T. Hung, *The natural synovial joint: properties of cartilage*, Proc. Inst. Mech. Eng. Part J: J. Eng. Tribol., 220 (2006), pp. 657–670.

[4] E. A. Balazs, *The role of hyaluronan in the structure and function of the biomatrix of connective tissues*, Struct. Chem., 20 (2009), pp. 233–243.

[5] N. J. Balmforth, C. J. Cawthorn and R. V. Craster, *Contact in a viscous fluid. Part 2. A compressible fluid and an elastic solid*, J. Fluid Mech., 646 (2010), pp. 339–361.

[6] G. S. Beavers and D. D. Joseph, *Boundary conditions at a naturally permeable wall*, J. Fluid Mech., 30 (1967), pp. 197–207.

[7] C. J. Cawthorn and N. J. Balmforth, *Contact in a viscous fluid. Part 1. A falling wedge*, J. Fluid Mech., 646 (2010), pp. 327–338.
[8] S. H. Davis and L. M. Hocking, *Spreading and imbibition of viscous liquid on a porous base*, Phys. Fluids, 11 (1999), pp. 48–57.
[9] H. Fam, J. T. Bryant and M. Kontopoulou, *Rheological properties of synovial fluids*, Biorheology, 44 (2007), pp. 59–74.
[10] S. L. Goren, The hydrodynamic force resisting the approach of a sphere to a plane permeable wall, J. Colloid Interface Sci., 69 (1979), pp. 78–85.
[11] J. S. Hou, V. C. Mow, W. M. Lai and M. H. Holmes, *An analysis of the squeeze-film lubrication mechanism for articular cartilage*, J. Biomech., 25 (1992), pp. 247–259.
[12] M. B. Jones, G. R. Fulford, C. P. Please, D. L. S. McElwain and M. J. Collins, *Elastohydrodynamics of the eyelid wiper*, Bull. Math. Biol., 70 (2008), pp. 323–343.
[13] J. R. Lin, R. F. Lu and C. B. Yang, *Derivation of porous squeeze-film Reynolds equations using the Brinkman model and its application*, J. Phys. D: Appl. Phys., 34 (2001), pp. 3217–3223.
[14] D. A. Nield and A. Bejan, *Convection in Porous Media*, 3rd Edition, Springer (2006), pp. 17–21.
[15] D. A. Nield, *The Beavers–Joseph boundary condition and related matters: a historical and critical note*, Transp. Porous Media, 78 (2009), pp. 537–540.
[16] A. Nir, *On the departure of a sphere from contact with a permeable membrane*, J. Eng. Math., 15 (1981), pp. 65–75.
[17] K. Nong and D. M. Anderson, *Thin film evolution over a thin porous layer: modeling a tear film on a contact lens*, SIAM J. Appl. Math., 70 (2010), pp. 2771–2795.
[18] N. Nuño and A. M. Ahmed, *Three-dimensional morphometry of the femoral condyles*, Clin. Biomech., 18 (2003), pp. 924–932.
[19] B. P. O'Hara, J. P. G. Urban and A. Maroudas, *Influence of cyclic loading on the nutrition of articular cartilage*, Ann. Rheum. Dis., 49 (1990), pp. 536–539.
[20] J. Prakash and S. K. Vij, *Load capacity and time-height relations for squeeze films between porous plates*, Wear, 24 (1973), pp. 309–322.
[21] J. Prakash and S. K. Vij, *Effect of velocity slip on porous-walled squeeze films*, Wear, 29 (1974), pp. 363–372.
[22] J. D. Sherwood, *The hydrodynamic forces on a cylinder touching a permeable wellbore*, Phys. Fluids A, 2 (1990), pp. 1754–1759.
[23] J. M. Skotheim and L. Mahadevan, *Soft lubrication: the elastohydrodynamics of nonconforming and conforming contacts*, Phys. Fluids, 17 (2005), 092101.
[24] S. Standring (Ed.), *Gray's Anatomy*, 40th Edition, Churchill Livingstone (2008), Chapter 82, pp. 1393–1410.
[25] T. Stewart, Z. M. Jin and J. Fisher, *Friction of composite cushion bearings for total knee joint replacements under adverse lubrication conditions*, Proc. Inst. Mech. Eng. Part H: J. Eng. Med., 211 (1997), pp. 451–465.
[26] H. A. Stone, *On lubrication flows in geometries with zero local curvature*, Chem. Eng. Sci., 60 (2005), pp. 4838–4845.
[27] A. Z. Szeri, *Fluid Film Lubrication*, Cambridge University Press (1998).
[28] P. S. Walker, G. Yildirim, S. Arno and Y. Heller, *Future directions in knee replacement*, Proc. Inst. Mech. Eng. Part H: J. Eng. Med., 224 (2010), pp. 393–414.
[29] S. J. Weekley, S. L. Waters and O. E. Jensen, *Transient elastohydrodynamic drag on a particle moving near a deformable wall*, Q. J. Mech. Appl. Math., 59 (2006), pp. 277–300.
[30] E. W. Weisstein, *Lambert W-Function*, `mathworld.wolfram.com/LambertW-Function.html`, accessed on 25th April 2012.
[31] H. Wu, *Squeeze-film behaviour for porous annular disks*, J. Lubr. Technol., 92 (1970), pp. 593–596.
[32] H. Wu, *Effect of velocity-slip on the squeeze film between porous rectangular plates*, Wear, 20 (1972), pp. 67–71.

RECENT REPORTS

12/18	A note on oblique water entry	Moore Howison Ockendon Oliver
12/19	Calculus on surfaces with general closest point functions	März Macdonald
12/20	Multiple equilibria in a simple elastocapillary system	Taroni Vella
12/21	Multiphase modelling of vascular tumour growth in two spatial dimensions	Hubbard Byrne
12/22	Chebfun and Numerical Quadrature	Hale Trefethen
12/23	Moment-based formulation of NavierMaxwell slip boundary conditions for lattice Boltzmann simulations of rarefied flows in microchannels	Reis Dellar
12/24	Correspondence between one- and two-equation models for solute transport in two-region heterogeneous porous media	Davit Wood Debenest Quintard
12/25	Rolie-Poly fluid flowing through constrictions: Two distinct instabilities	Reis Wilson
12/26	Age related changes in speed and mechanism of adult skeletal muscle stem cell migration	Collins-Hooper Woolley Dyson Patel Potter Baker Gaffney Maini Dash Patel
12/27	The interplay between tissue growth and scaffold degradation in engineered tissue constructs	ODea Osborne El Haj Byrne Waters
12/28	Non-linear effects on Turing patterns: time oscillations and chaos.	Aragon Barrio Woolley Baker Maini
12/29	Colorectal Cancer Through Simulation and Experiment	Kershaw Byrne Gavaghan Osborne
12/30	A theoretical investigation of the effect of proliferation and adhesion on monoclonal conversion in the colonic crypt	Mirams Fletcher

12/33	Second weak order explicit stabilized methods for stiff stochastic differential equations	Abdulle Vilmart Zygalakis
12/34	The sensitivity of Graphene 'Snap-through' to substrate geometry	Wagner Vella
12/35	The physics of frost heave and ice-lens growth	Peppin Style
12/36	Finite Element Simulation of Dynamic Wetting Flows as an Interface Formation Process	Sprittles Shikhmurzaev
12/37	The Dynamics of Liquid Drops and their Interaction with Solids of Varying Wettabilities	Sprittles Shikhmurzaev
12/38	Dispersal and noise: Various modes of synchrony in ecological oscillators	Bressloff Lai
12/39	Boundary conditions for free surface inlet and outlet problems	Taroni Breward Howell Oliver
12/40	A Branch and Bound Algorithm for the Global Optimization of Hessian Lipschitz Continuous Functions	Fowkes Gould Farmer
12/41	The Orthogonal Gradients Method: a Radial Basis Functions Method for Solving Partial Differential Equations on Arbitrary Surfaces	Piret

Copies of these, and any other OCCAM reports can be obtained from:

Oxford Centre for Collaborative Applied Mathematics
Mathematical Institute
24 - 29 St Giles'
Oxford
OX1 3LB
England
www.maths.ox.ac.uk/occam